論文 / 著書情報
Article / Book Information

Title	A Mohr-Coulomb-Vilar model for constitutive relationship in root-soil interface under changing suction
Authors	Haruka Tomobe, Kazunori Fujisawa, Akira Murakami
Citation	Soils and Foundations, Volume 61, Issue 3, Page 815-835
Pub. date	2021, 6

HOSTED BY

ELSEVIER

Available online at www.sciencedirect.com

ScienceDirect

Soils and Foundations 61 (2021) 815–835

SOILS AND FOUNDATIONS

www.elsevier.com/locate/sandf

Technical Paper

A Mohr-Coulomb-Vilar model for constitutive relationship in root-soil interface under changing suction

Haruka Tomobe *, Kazunori Fujisawa, Akira Murakami

Graduate School of Agriculture, Kyoto University, Japan

Received 5 November 2019; received in revised form 18 February 2021; accepted 7 March 2021
Available online 21 May 2021

Abstract

Understanding mechanical interactions at the root-soil interface is essential to predict the erosion of vegetated slopes. Recently, the shear strength of vegetatedil under changing hydraulic conditions has been measured and modeled; however, root-soil interfaces have not been investigated under changing hydraulic conditions. This paper proposes (1) a novel pullout apparatus to measure the shear strength at the root-soil interface under changing suction, (2) a Mohr-Coulomb-Vilar (MCV) shear strength model of root-soil interfaces, and (3) a numerical simulation using Node-To-Segment (NTS) approach along with Finite Element Method (FEM). The pullout tests were verified using the numerical simulation, and the results showed that the combination of the MCV model and NTS/FEM approach can accurately predict the shear behavior of root-soil interfaces under changing suction. In addition, we experimentally evaluated the pullout problem of roots and showed that the present method provides reasonably predicts root-pullout problems even when the suction is changed during the pullout process. The current method, therefore, can be used for predicting root-soil interface dynamics under varying suction and soil pressure by only adding two additional parameters of the Vilar model.

Keywords: Pull-out tests; Shear strength; Root-soil interface; Suction; Mohr-Coulomb-Vilar model; Node-To-Segment approach

1. Introduction

Plant roots increase the shear strength of soil mass; hence, it is essential to understand and estimate the mechanical interactions between roots and soil in order to predict the erosions of vegetated slopes. As roots reinforce the soil mass, rooted soil has a higher shear strength than soil alone (Mickovski et al., 2011). This reinforcement can be measured by direct shear tests (Abe and Zimemer, 1991; Eab et al., 2015; Wood et al., 2017; Liang et al., 2017; Pallewattha et al., 2019), which show that the cohesion and friction increase in rooted soil due to the tensile strength of roots and the shear strength of root-soil interfaces. A similar phenomenon has been observed in fiber-reinforced soils (Ghavami et al., 1999; Ibraim et al., 2010). In both cases, the contribution of the fiber tensile strength increases the shear and tensile strength of the mixture. For this reinforcement to take effect, the soil and fiber must be in contact; therefore, the condition of the soil-fiber contact surface in the mixture is a key factor determining the magnitude of this reinforcement effect. Consequently, understanding the mechanical interactions between roots and soil is essential for predicting and preventing landslides and the erosion of vegetated slopes.

Humidity is a primary factor determining the shear strength of rooted soil; therefore, the hydromechanical properties of rooted soil have been investigated for decades (Fan et al., 2008, 2009; Ng et al., 2013; Kamchoom and Leng, 2018). The shear strength of rooted soil has been investigated by direct shear tests (Endo, 1980; Abe and

* Corresponding author.
E-mail addresses: tomobe@toyota-ct.ac.jp (H. Tomobe), fujik@kais.kyoto-u.ac.jp (K. Fujisawa), akiram@kais.kyoto-u.ac.jp (A. Murakami).

https://doi.org/10.1016/j.sandf.2021.03.005
0038-0806/

Ziemer, 1991, Fan et al., 2009; Ni et al., 2018) on disturbed or undisturbed samples. The results suggest that the Mohr–Coulomb (MC) model can describe the shear strength of rooted soil, where the root reinforcement primarily appears in the apparent cohesion and secondary apparent frictional angle. This mechanical reinforcement effect is also strongly influenced by the moisture retention conditions in the soil. For instance, Fan et al. (2009), Ni et al. (2018), Mahannopkul and Jotisankasa (2019) reported that the increased suction can enhance the apparent cohesion and friction angle of rooted soil. The authors explained that the soil domains are divided and covered by root fibers and that the roots protect soil domains from water penetration. One of the characteristic functions of plant roots is the ability to absorb water from the soil. This function dramatically alters the water retention conditions in the soil. Ng et al. (2013) and Kamchoom and Leng (2018) experimentally and numerically showed that transpiration and fibrous roots increase slope stability in vegetated slopes. Although these experimental observations have led to simple mechanical models of the shear strength of rooted soil under changing hydromechanical conditions, further investigations are required to provide accurate predictions and numerical models of the shear strength of rooted soil for the design and preservation of vegetated slopes (Giadrossich et al., 2017).

Plant roots transform the pore-structure and hydraulic field of soil, thereby changing its hydraulic conductivity and water content (Ng et al., 2013; Leung et al., 2015; Song et al., 2017; Ni et al., 2019). As reported by Ng et al. (2013), the plant-induced suction caused by evapotranspiration and water-absorption of plants is the primary cause of root reinforcement. Such plant activities reduce the water content of soil and hence increase the soil shear strength. Furthermore, roots change the hydraulic conductivity, and lower the soil water content (Song et al., 2017). It has been hypothesized that the reduced shear strength of rooted soil observed in the presence of high water content is primarily caused by a loss of shear strength among soil domains in rooted soil. However, it remains unclear how changes in the hydraulic conditions of the microscopic root-soil interface affect the macroscopic soil shear strength.

Because rooted soil consists of roots and soil, the hydromechanical response of root-soil interfaces, especially the shear strength and suction of root-soil interfaces may play a critical role in the bulk shear strength of rooted soil under changing hydraulic conditions. The shear strength of root-soil interfaces has been evaluated by pullout tests, which can measure the friction and cohesion of the interfaces with respect to unsaturated root-soil interfaces (Voottipuex et al., 2008; Bischetti et al., 2010; Schwarz et al., 2011; Hejazi et al., 2012; Ji et al., 2018; Tomobe et al., 2019). Previous studies have been based on two different strategies. In the first strategy, one examines theroot pullout resistance from a macroscopic standpoint (Hejazi et al., 2012; Ji et al., 2018; Pallewattha et al., 2019). This approach provides important information because it directly measures the pull-out resistance of the roots and is easy to understand from a macroscopic vewpoint. In the second approach, one investigates the microscopic relationship between the shear strength of the root-soil contact surface and the contact surface conditions (Mickovski et al., 2009; Bischetti et al., 2010; Tomobe et al., 2016, 2019). The microscopic shear characteristics of root-soil interfaces are essential for finite element (FE)-analysis (Mickovski et al., 2009; Tomobe et al., 2019). These investigations have utilized pullout tests to estimate the shear strength of root-soil interfaces and have shown that the MC model can model the interfacial shear strength. However, it is difficult to utilize these conventional models to predict the shear strength of root-soil interfaces under changing soil pressure and suction.

In this work, we propose a series of methods to measure, model, and predict the shear strength of root-soil interfaces under changing soil-pressure and suction based on the pullout tests of Tomobe et al. (2016),Tomobe et al., 2019, the MC model (Tomobe et al., 2019), and the Vilar model (Vilar, 2006). Fig. 1 presents a schematic of major driving factors that influence the shear strength of root-soil interfaces. Friction increases with soil pressure, and interfacial root-soil cohesion increases under high-suction conditions. This soil-pressure-induced friction has been measured and modeled by Tomobe et al. (2016),Tomobe et al., 2019; however, suction-induced cohesion has not yet been studied (Table 1). In Sections 2 and 3 we present friction and suction-induced cohesion measurements, respectively. In Section 2, the pullout tests of Tomobe et al. (2016) are explained in detail because the original paper was written in Japanese and the content is closely related to an experiment proposed in Section 3 and numerical simulation presented in Section 5. Section 3 includes a novel pullout test for measuring the suction-induced cohesion of root-soil interfaces. As the shear strength of root-soil interfaces primarily arises from friction and cohesion, friction is modeled by the MC model, and cohesion is modeled by the Vilar model in this work. In Section 4, the MC model and Vilar model are merged as the MC-Vilar (MCV) model, which is implemented in numerical simulations based on the node-to-segment (NTS) method. The MCV-NTS method is validated by investigating numerical simulations of pressure-controlled and suction-controlled pullout tests in Section 5. The pullout of straight roots under varying suction is demonstrated in Section 6 to validate the applicability of the MCV-NTS scheme. Finally, the conclusions are given in Section 7.

2. Pressure-controlled pullout tests

2.1. Experimental procedure

This section briefly summarizes the pullout test method reported by Tomobe et al. (2016), which is described in a Japanese paper. The objective of the pullout test is to

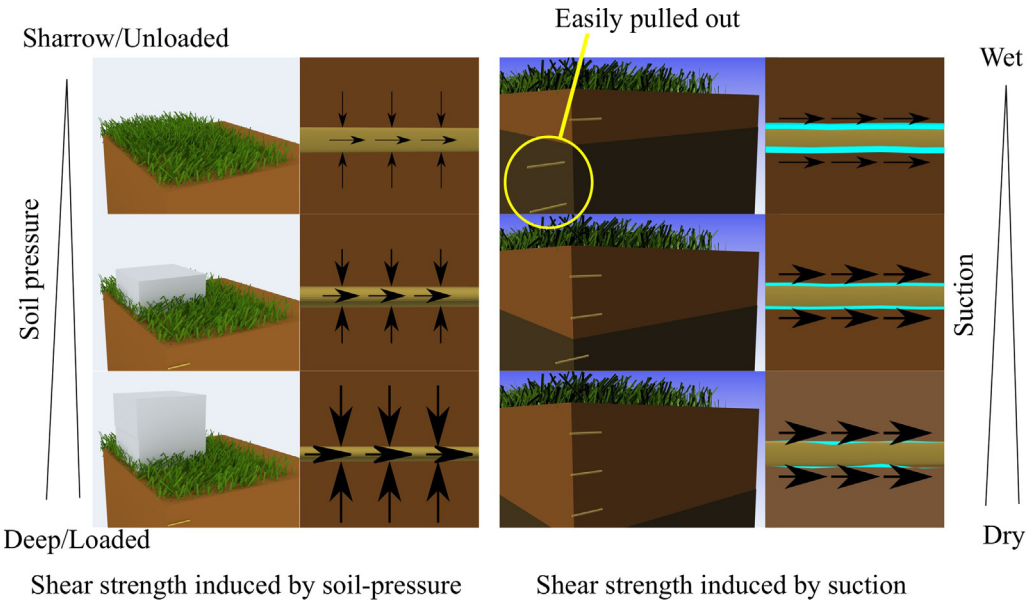

Fig. 1. Schematic view of two major driving factors of shear strength at the root-soil interface; soil pressure-induced friction (left) and suction-induced cohesion (right). Friction increases as the increase of soil pressure, and cohesion at the root-soil interface is increases under high-suction conditions.

Table 1
Structure of the present paper and the overview of the sections.

	Soil Pressure	Suction	Both
Experiment and model	Tomobe et al. (2016, 2019) Section 2	Novel apparatus Section 3	MCV model Section 4
Simulation	MCV-NTS approach Section 5		MCV-NTS for dynamic suction condition Section 6

measure the relationship between shear displacement and shear stress at a root-soil interface.

An apparatus was developed for measuring the shear behavior of root-soil interfaces. Fig. 2 displays a diagram of the pullout apparatus. As shown in the center of the figure, a straight root (diameter: 1.0 mm) is horizontally set on a steel soil box (diameter: 6.0 cm, thickness: 2.0 cm) through a set of holes (diameter: 0.5 cm), and soil is pou-

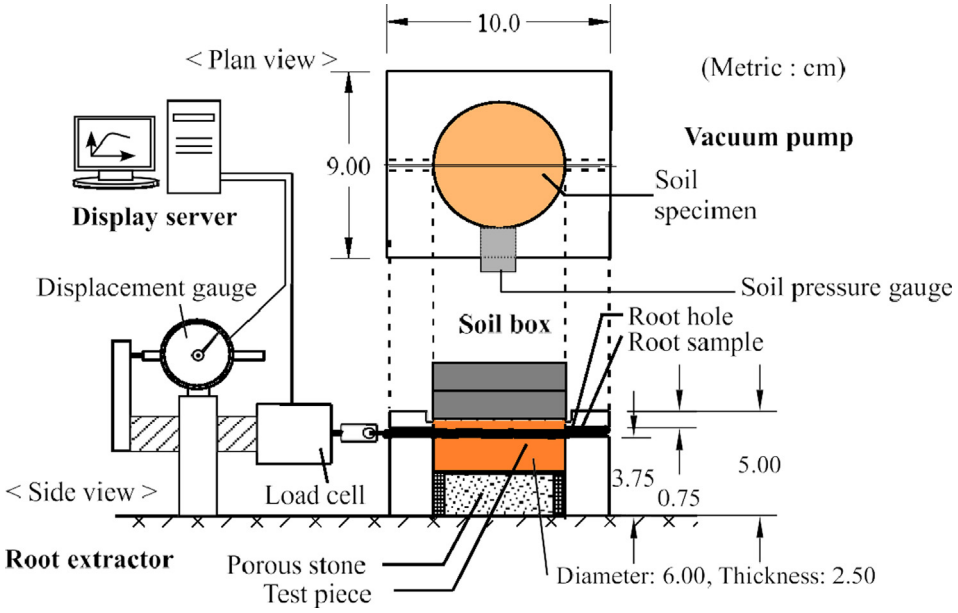

Fig. 2. Pullout apparatus for pressure-controlled pullout test for measuring the friction at the rootsoil interface.

blue into the soil box. Roots of the same diameter are used to ensure that the experimental conditions are uniform. It is well known that as roots grow, the epidermis changes in roughness and stiffness. Therefore, at different root diameters, the shear properties of the root-soil contact surface vary. Hence, for simplicity, only samples with a root diameter of 1 mm were used in this paper.The specimen is vertically compressed by the weight, and the root is pulled out to the left side of the figure at a speed less of than 0.1 mm/min, representing a pseudostatic condition. The reaction force is measublue by a forcegage and the horizontal displacement is measublue by a displacement gage attached to the left side of the force gage. During the pullout process, the horizontal soil pressure is measublue by a soil pressure gage attached to the side of the soil box. The soil pressure is used to compute the mean normal stress of the root-soil interface, which is identical to the soil pressure. In the present paper, the soil pressure is the normal stress indicated in the root-soil interfaces. The root is obtained from an experimental field at Kyoto University in Sakyo-Ku, Kyoto City, Japan (35°01′56.9″N, 135°47′00.9″E) containing barleys plants(*Hordeum vulgare L.*). The soil bulk density is 1.28 g/cm^3, the dry density of the soil is 0.97 g/cm^3, the soil water content is 31.5 % and the soil particle distribution is as shown in Fig. 3. The soil is categorized as SF-G based on JGS-0051–2009. It is worth noting that the dry density of the soil is low because the sampling site is a paddy field, where the soil is tilled and crops are planted. In addition, we assumed that the root diameter does not directly determine the shear strength of the root-soil interfaces; instead, the shear strength is determined by roughness, stiffness, and humidity. Because the present paper focuses on developing a novel methodology to measure the shear strength of root-soil interfaces under different suction conditions, parametric studies based on root diameter are leaft as future work. As shown in Fig. 4 the pullout test is performed as follows:

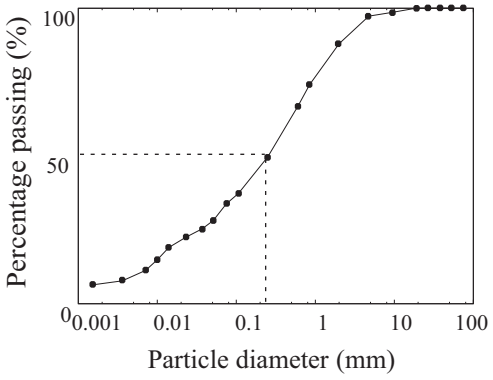

Fig. 3. Particle size distribution of soil material, which is same soil used by Tomobe et al. (2016).

1. A root segment is sampled from barleyroots, where a root without branch roots is chosen. The root is washed and tied to the force gage by a cotton string. The edge of the root is coveblue by wet papers to prevent drying. The water content of the paddy soil is set as 31.5 %, which is the same as that of the sampling site.
2. Paddy soil is poublue into the soil box to achieve a bulk density of 1.28 g/cm^3. The soil material is divided into four layers, and carefully filled and compacted by using a steel cylinder (diameter: 6.0 cm, thickness: 6.0 cm). The top of the soil surface is flattened by a soil knife. The soil box volume and soil water content are measublue beforehand, and the soil is confirmed to have a bulk density of 1.28 g/cm^3. The soil is poublue into the boxes four times, and each time the soil is uniformly compacted to meet the prescribed wet density. Soil test specimens are prepablue by the above procedure to meet the pblueetermined bulk density of 1.28 g/cm^3.

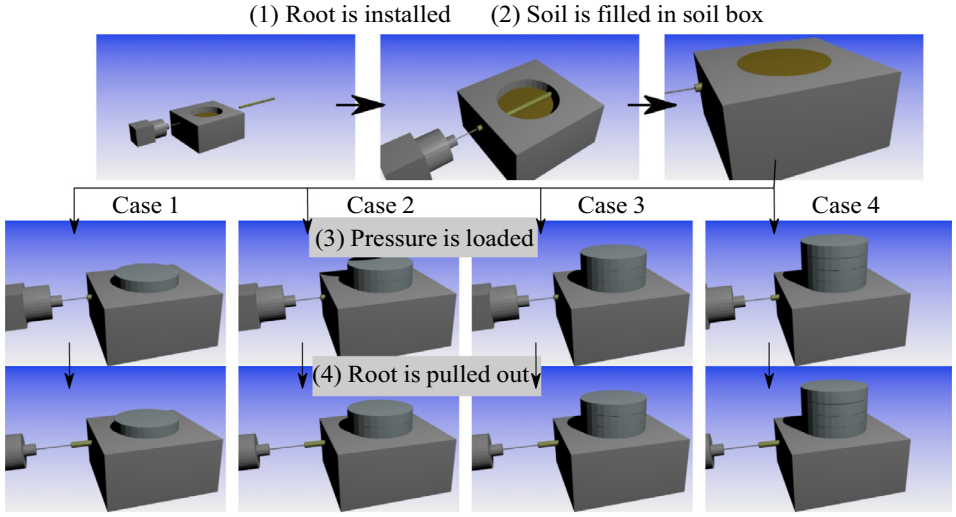

Fig. 4. Protocol of pressure-controlled pullout test: (1) a straight root is installed into an empty soil-box, (2) soil is filled into the soil-box, (3) prescribed pressures are loaded for Case 1 to 4, the mean soil pressure of the cases are 1.7, 3.6 6.1 and 8.3 kPa, respectively. (4) The root is pulled out by a displacement-controlled manner from the soil and reaction force is measured. During the pullout process, the vertical pressure is controlled.

3. Weights are placed on the soil specimen. The vertical displacement of the soil surface is measublue until the deformation stops, which occurs after more than 20 min. Steps 1–3 are conducted four times (Cases 1,2,3, and 4) under different soil pressures (1.7, 3.6, 6,1 and 8.3 kPa). The stress is equivalent to the typical pressure of the surface soil (depth: 0.1–1.0 m) into which plant roots penetrate.
4. After the deformation stops, the root specimen is pulled out at a speed of 0.1 mm/min over 6.0 mm. During the pullout process, profiles of the horizontal soil pressure (kPa), pullout force (N), and horizontal displacement (mm) are measublue.

The soil density is carefully controlled by static compaction as follows

1. Precisely measure the volume of the soil box.
2. Measure the density of soil particles based on JIS A 1204.
3. Calculate the soil mass to be placed in the soil box based on the soil particles density and soil box volume.
4. Add water to achieve a predetermined water content ratio.
5. Disturb the soil to make it larger than the volume of the soil box.
6. Divide the soil sample into exactly three equal portions, place one of the portions in the container, and statically compact it up toexactly one-third the height of the soil box.
7. Perform the previous procedure in (6) three times to achieve the exact dry density in the container

After the experiment, the water content (%), and dry density (g/cm^3) are measured. The soil pressure and shear stress of an interface are estimated by $\sigma_N = (\sigma_1 + \sigma_2)/2$, where σ_1 is the vertical soil pressure induced by weight and σ_2 is the horizontal soil pressure measublue by the soil pressure gage. This equation is derived from the following mathematical operations. Let us utilize Cauchy's stress tensor σ of the soil as below.

$$\sigma_N = \frac{1}{2\pi rL}\int_A \sigma \mathbf{n}\cdot\mathbf{n} dA \tag{1}$$

with,

$$\sigma = \begin{pmatrix} \sigma_1 & 0 & 0 \\ 0 & \sigma_2 & 0 \\ 0 & 0 & \sigma_2 \end{pmatrix} \tag{2}$$

$$\mathbf{n} = \begin{pmatrix} \cos\theta \\ \sin\theta \\ 0 \end{pmatrix} \tag{3}$$

where $\mathbf{n}$ is the unit outer vector normal to the interface on the pullout material surface, θ is changed from 0 degrees to 2π degrees, σ_N is the soil pressure on the pullout material, r and L are the mean radius (m) and length (m) of the pullout material, respectively, π is a circle ratio, and A is the area of the interface (m^2). The root samples can be modeled as a cylinder; thus Eq. (1) can be computed and $\sigma_N = (\sigma_1 + \sigma_2)/2$ is obtained.

Similarly, the shear stress of the root-soil interface is computed by Eq. (4):,

$$\tau = \frac{S}{2\pi rL}, \tag{4}$$

where S is the pullout resistance.Importantly the shear stress in Eq. (4) is an area-averaged value, as used in Eq. (1). The average shear stress is derived by an area-averaging process smilar to that employed in Eq. (1).

Furthermore, We note that the soil water retention curve provides important information regarding unsaturated soil properties. However, this information is not directly related to the MCV model proposed in this study, and it is difficult to measure soil water retention curves under the extremely low soil pressure used in this study. Therefore, soil water retention curves were not outmeasublue in this study.

2.2. Relationship between shear behavior and soil pressure of root-soil interfaces

Table 2 shows the dry density and water content of the soil measublue after the experiments. For all cases, the initial dry density is 0.97 g/cm^3, and the water content is 31.5 %.

After the experiment, the dry density ranges between 0.96 g/cm^3 and 0.98 g/cm^3, remaining almost the same in all cases. Notably, the bulk density and dry density of the soil are calculated by dividing the dry weight by the initial volume. Hence, the densities determined during the pullout process are larger than those measublue after the experiment.

The water content does not change significantly; thus, the mechanical properties of the soils do not change significantly during the experiment, as the soil pressure is negligible.

The relationship between shear displacement and shear stress under varying normal stress is shown in Fig. 5. The shear stress is proportional to the shear displacement when the shear displacement is less than 4.0 mm. The shear stress increases as the shear displacement increases to approximately 4.0–7.0 mm, reaching the maximum shear stress.

Table 2
Material properties of soil sample.

Soil particle density (g/cm^3)	2.67
Dry soil density (g/cm^3)	0.97
Bulk soil density (g/cm^3)	1.28
Water content (%)	31.5
Maximum root diameter (mm)	0.74
minimum root diameter (mm)	0.68

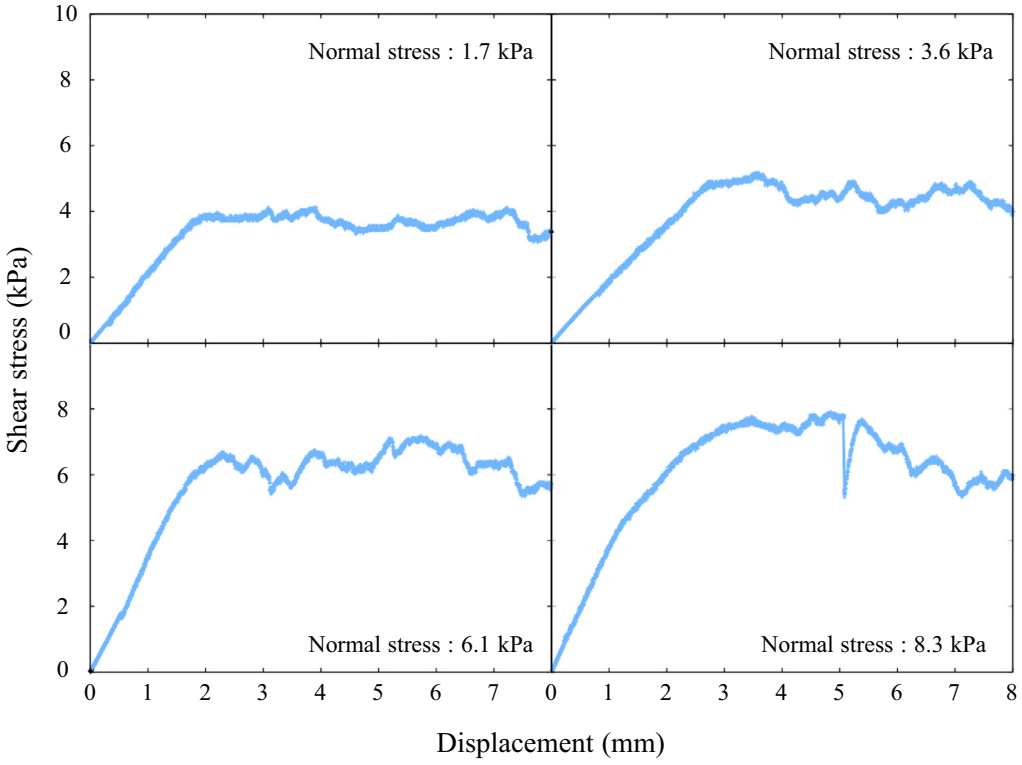

Fig. 5. Relationship between shear displacement and shear stress measured by pressure-controlled pullout tests for normal pressures of root-soil interface 1.7, 3.6 6.1 and 8.3 kPa, respectively.

After the peak shear stress is observed, the shear stress remains nearly the same over the range of 2.0–5.0 mm. The relationship between the normal stress and maximum shear stress is shown in Fig. 6. The maximum shear stress is proportional to the normal stress ($R^2 = 0.98$). The intercept of the line is 3.14 kPa and the frictional coefficient is 0.60. This relationship is consistent with the well-known MC model and the coefficients are consistent with the frictional coefficient; hence, the friction coefficient between the root and the soil is 0.60. The friction angles measublue by Schwarz et al. (2011) ranged from 0.46 to 0.70, which is consistent with the friction angle measublue in the present work.

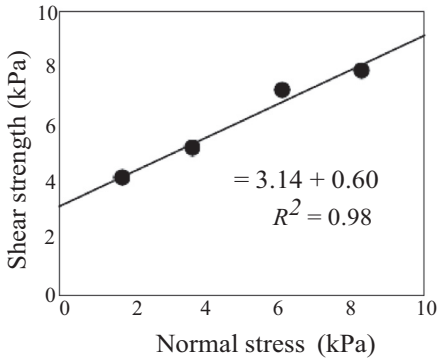

Fig. 6. Relationship between normal stress and shear strength of root-soil interface measured by pressure-controlled pullout tests: Mohr–Coulomb criterion is applicable to the slip criterion.

3. Suction-controlled pullout test

3.1. Apparatus and procedure

A suction-controlled pullout test aims to measure the shear properties of root-soil interfaces under a prescribed suction. For this purpose, a novel pullout apparatus was developed, which consists of a soil box, vacuum pump, root extractor, and display server (Fig. 7). The soil box, root extractor, and display server are the same as those used in the pullout apparatus presented by Tomobe et al. (2016), but the vacuum pump (DIK-9230 Automatic Pressure Controller, DAIKI RIKA KOGYO, Japan) is a new addition, included to control the suction of the soil box. The vacuum pump can maintain pressures of 0 kPa to −30.0 kPa, which is satisfactory for this experiment.

The root specimens were sampled from barley plants (Hordeum vulgare L.) cultivated in Kyoto city, Japan (35 ° 01'57.2"N, 135 ° 47'00.4"E) in 2015, as used in the work by Tomobe et al. (2016). Ten barley plants and the surrounding soil were sampled from the site. The plants and soil were carefully separated without changing the water content. The soil was sieved with a 2.0 mm sieve, and the soil that passed through the sieve was utilized for the experiments. The soil was coveblue with plastic wrap to prevent drying. Ten roots were selected and sampled from the plants. Each root was straight and smooth and had a roughly constant diameter, as shown in Table 2. The soil was sampled from the surface layer (0 to −15 cm) of the

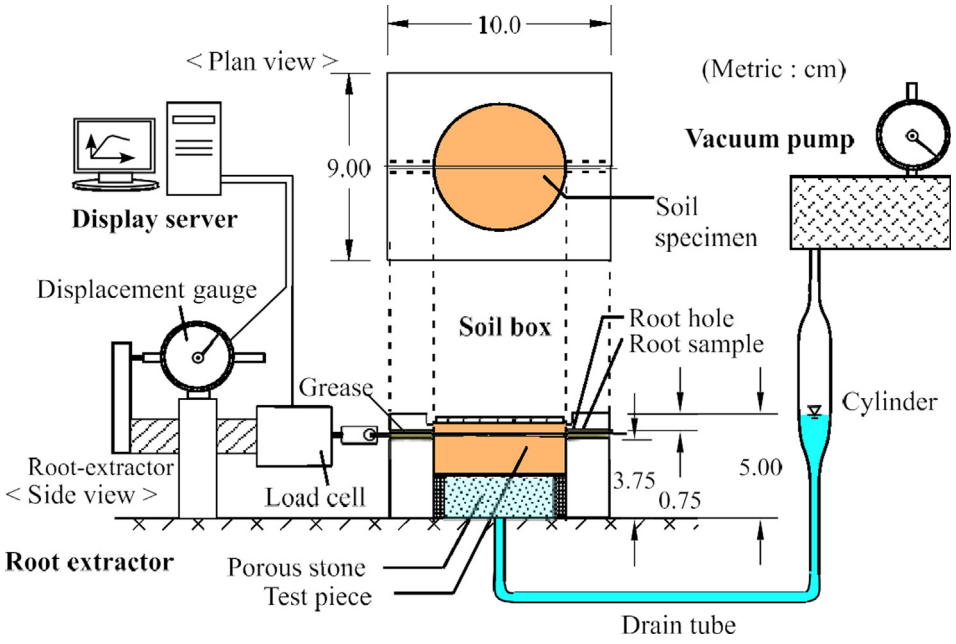

Fig. 7. Apparatus for suction-controlled pullout tests: Suction is loaded by (right) vacuum pump and no soil pressure is loaded.

cultivated field after the roots were obtained; at the same time, undisturbed soil samples were collected to measure the bulk density, water content, grain size, and soil particle density (see Table 2 and Fig. 3). The soil properties were the same as those for the experiment reported in Section 2. The soil is categorized as sandy silt according to the geomaterial classification method for engineering purposes (JGS 0051–2009).

The procedure of the experiment is shown in Fig. 8. Before the experiment, the root hole was filled with greaseto block water, and the drain tube, porous stone, and soil box were carefully saturated with water. A porous stone mounted in a compact-type direct shear apparatus (MIS-233–1-04, MARUI & CO., Ltd.) was utilized in the experiment. Although air-entry value (AEV) data for the porous stone were not presented, the authors confirmed that the AEV is sufficient to load the suction. Notably, the porous stone is crimped and coated by kaolin clay beforehand. As reported by Wijaya et al. (2015), the specimen made by kaolin clay has an AEV of 356 kPa, which exceeds 30 kPa requiblue in this study.

Subsequently, the roots and soil were placed in the soil box, at a dry bulk density equal to that for one of the sampling points. Then, the pump suctioned the water at a prescribed pressure, and the water began to move from the soil specimen to the cylinder until an equilibrium was achieved. The equilibrium is varified by measuring the water level in the cylinder. During the process, a thin plastic cover is placed on the soil specimen to prevent drying. In this experiment, the normal stresses are zero because the normal pressure on the root-soil interface is negligibly small. Notably, this test focuses on measuring the pure apparent cohesion induced by suction; therefore, the vertical stress should be minimized. The soil-pressure induced friction was measublue as described in the previous sections, and both the friction and cohesion were utilized for the MCV model to model realistic conditions.

After equilibrium was achieved, the root was slowly (less than 0.1 mm/min) pulled out from the soil box by the root extractor, as shown in Fig. 7. the reaction force and the horizontal displacement are measublue until the shear stress reached a peak. This reaction force was measublue by a load cell (LUX-B-50 N-ID, KYOWA ELECTRONIC INSTRUCTION, Japan) and the displacement was recorded by using the displacement gage (DDP-20A, Tokyo Sokki Kenkyujo, Japan). This process was repeated for six cases under different suction conditions (0.5, 4.4, 5.8, 8.8, 22.0, and 28.0 kPa). These suction level were chosen because the maximum possible suction realized by the apparatus is 28.0 kPa under atmospheric pressure,ranging from water-saturated conditions to field water capacity. The corresponding water content by mass for each case was, 57.15, 37.06, 38.29, 29.74, 29.73, and 23.91 %, respectively. No vertical stress was loaded in any of the exeriments, in order to observe the pure suction-induced cohesion. Parametric studies of simultaneous vertical-stress and suction loading are left as future work due to the following technical difficulties: (1) A duration of 24 to 72 h is needed to conduct suchthe experiments when the suction is greater than 10 kPa; therefore, if four or more vertical stress conditions are evaluated, the experiments will last 1–2 weeks. It is technically difficult to ensure that the soil water content, structure, and other properties remain constant for such a long time. (2) The plant roots mustalso be stoblue, however, it is difficult to maintain living plants and/or roots for more than one week.

The profile of the shear stress in the root-soil interfaces was obtained by dividing the total pullout force by the

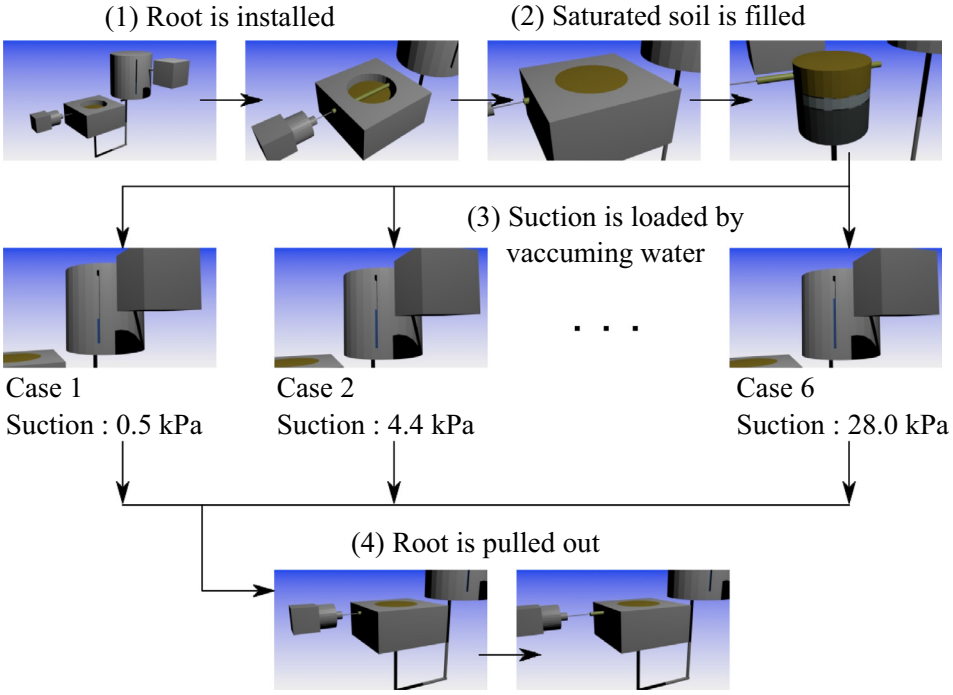

Fig. 8. Protocol of suction-controlled pullout tests: (1) a straight root is installed into an empty soil-box, (2) water-saturated soil is filled into the soil-box, (3) prescribed suctions are loaded for Case 1 to Case 4, where the soil suction are 0.5, 4.4, 5.8, 8.8, 22.0, and 28.0 kPa, respectively. (4) The root is pulled out from the soil and reaction force is measured.

surface area of the root segment. Hence, the shear stress was computed by Eq. (4). We note that this simple relationship can be used only when the diameter of the root segment is nearly constant and branch roots are not present; therefore, the root segments were sampled from straight roots with no branches or the root hair.

The relationship between suction and shear strength was plotted to evaluate the shear reinforcement in the root-soil interface due to suction. Based on the relationship between the suction-induced cohesion and suction, a model was proposed for FE method (FEM) analysis. Similar relationship have been obtained for the cases of soil-soil interfaces (Likos et al., 2018) and geotextile-soil interfaces (Jotisankasa and Rurgchaisri, 2018) with corresponding models available for FEM analysis, however, the relationship has not been measublue or modeled for root-soil interfaces. This paper models the strength-suction curve based on the formulation of Vilar (2006), which has been utilized for modeling suction-induced cohesion in unsaturated soil.

3.2. Relationship between shear behavior and suction of root-soil interfaces

Shear stress profiles were measured by pullout tests for each experimental casem as shown in Fig. 9. The curves primary show that the shear stress increases with increasing displacement and asymptotically approaches the maximum shear stress. Severalpreliminary tests were performed when the root-samples were fresh, however, onlycases (e) and (f) show results for roots that have not broken. Therefore, in realistic conditions, root breakage can be essential when the suction-induced cohesion reaches high levels. Because both root breakage and root slippage can be observed in actual phenomena, it is desirable to use the present model in combination with a root-breakage model. Although few root-breakage models have been validated, it is thought that breakage models of artificial materials can be used, such as Jin et al. (2019) or Sugiman et al. (2011). These models suggest that the shear stress initially increases at a constant rate for displacements of 0.0–5.0 mm and then remains constant for displacement of 5.0–18.0 mm. After the shear stress reaches the shear strength, the roots globally slip, followed by a moderete [Cases (a), (b) and (c)] or rapidl [Cases (d), (e) and (f)] decrease in stress. Compared with the curve for Case (a), where the suction is almost 0 kPa, the stiffness and shear strength of the root-soil interfaces are much larger for the other cases, and the suction-induced cohesion in the root-soil interface increases significantly from 0 kPa to 20 kPa as the suction increases from 0.0 to 10.0 kPa. When the suction exceeds 10 kPa, the suction-induced cohesion reaches approximately 25 kPa.

The relationship between the maximum shear stress and suction is shown in Fig. 10. The shear strength increases with increasing for suction values below 10.0 kPa; for larger suction values, the shear strength reaches a constant value. Similar responses have been observed for geotextile-soil interfaces (Jotisankasa and Rurgchaisri, 2018) and soil-soil interfaces (Song et al., 2017). However, to the best of our knowledge, This paper is the first report

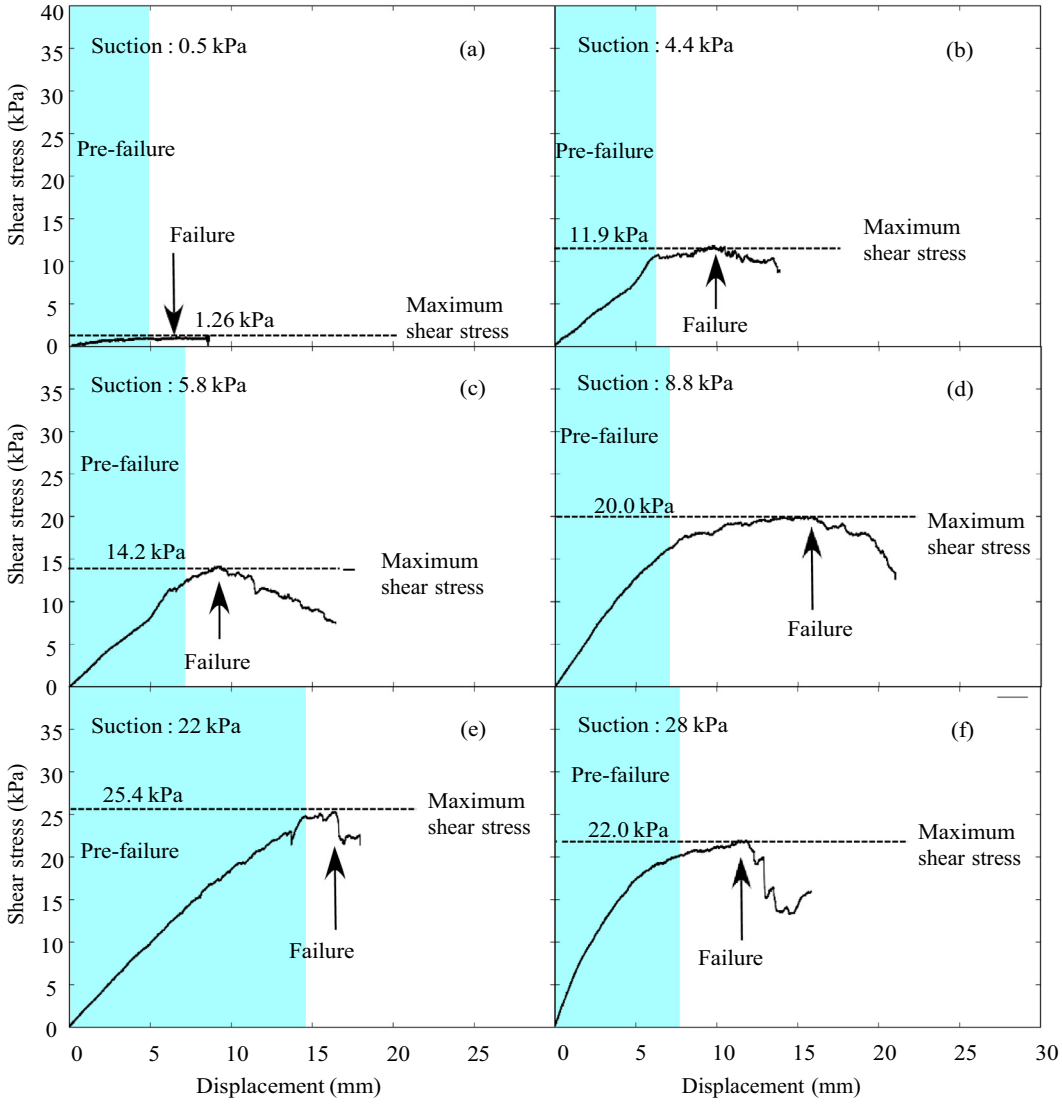

Fig. 9. Relationship between shear displacement and shear stress measured by -controlled pullout tests for suctions of root-soil interface 0.5, 4.4, 5.8, 8.8, 22.0, and 28.0 kPa, respectively.

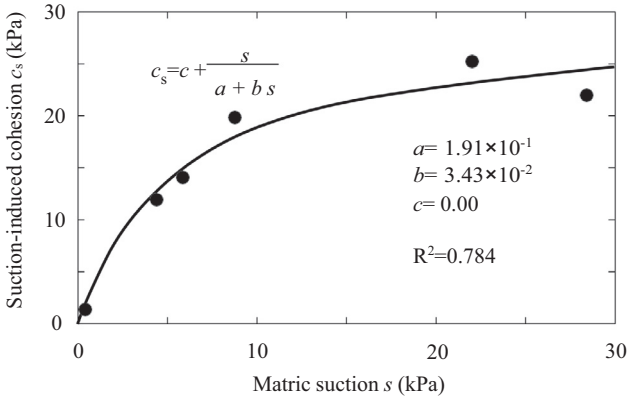

Fig. 10. Relationship between suction and shear strength of root-soil interface measured by suction-controlled pullout tests, and Parameter fitting of Vilar model for the Relationship between suction and shear strength of root-soil interface.

such a response for root-soil interfaces As shown in Fig. 10, the model of Vilar (2006) is used in this section to express the relationship between the suction and shear strength of root-soil interfaces. The Vilar model is also used to obtain model parameters, where the suction-induced cohesion is equal to the maximum shear stress. The model is expressed as

$$\tau = c + \frac{s}{a \cdot s + b} \tag{5}$$

where τ is the shear strength of the root-soil interface, s is the suction, c is the cohesion, and a and b are model parameters. This model was chosen for three reasons: (1) the mechanism of suction-induced reinforcements in soil-soil interfaces which are similar to root-soil interfaces, can be modeled by the Vilar model, as shown in Fig. 11. This model illustrates the hypothetical structure of

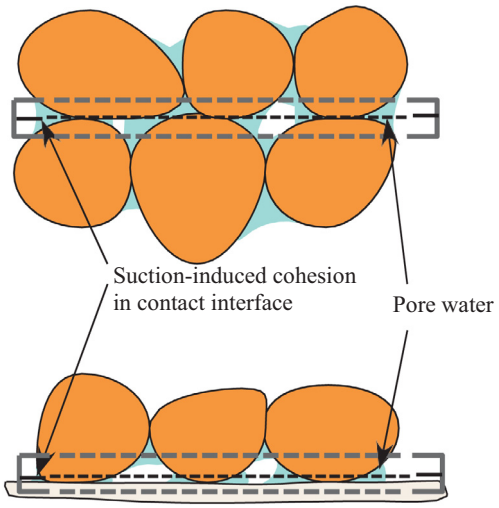

Fig. 11. Schematics of root-soil interface and soil-soil interface.

soil-soil and root-soil interactions under unsaturated conditions. Surface water can generate cohesion between soil particles; therefore, the same phenomena is expected to occur in root-soil interfaces. (2) This model can express nonlinearity with the simplest possible function. (3) In other methods, such as the method of Fredlund (1996), the effective angle of friction should be the same as the friction angle relative to the suction; however, in this case, the frictional angle estimated from the relationship between suction and shear strength is 68 degrees, which is significantly greater than the value obtained from frictional tests (Tomobe et al., 2016). The relationship between suction and suction-induced cohesion has been intensively investigated (Fredlund, 1996; Zhang et al., 2013; Likos et al., 2018). Such reports have suggested the existence of a suction-induced effective stress on soil particles. Theoretically, the effective stress due to suction should be proportional to the suction-induced cohesion, and the proportionality constant should be equal to the friction angle of the contact surface measured by direct shear tests (Fredlund, 1996). However, research have reported cases of fiber-soil contact in which these parameters are not equal at low restraint pressures (Likos et al., 2018), where it is suggested that the increased strength due to dilation may cause this phenomenon. The findings described in the present section are consistent with those reported by Likos et al. The results of curve fitting are presented in Fig. 10, and the parameters a and b are shown in Table 3, which can precisely express the suction-induced cohesion. In this case, the normal stresses is zero because the normal pressure on the root-soil interfaces is negligibly small during the experiment. The relationship shown in Fig. 10 is normalized with respect to the root diameter and the vertical stress as presented in Eqs. (1)–(4); therefore, it is natural to assume that the same coefficients can be consistently utilized for other root diameters and vertical stresses.

4. Constitutive modeling of shear strength of root-soil interfaces under changing pressure and suction

4.1. Mohr–Coulomb-Vilar model

In Section 3, the Vilar model was utilized along with the MC model to express the suction-induced cohesion of root-soil interfaces under different suction and stress conditions. Here, we develop the MCV model, in which the shear strength of a root-soil interfaces is expressed as

$$\tau_{max} = c + \mu \cdot \sigma_N + \frac{s}{a \cdot s + b} \tag{6}$$

where τ_{max} is the shear strength, μ is the frictional coefficient and σ_N is the soil pressure. In this model, root-slippage is considered; however, root breakage is not considered due to our focus on a constitutive model for root-soil interfaces. However, root breakage can be considered in a constitutive model for root-soil systes. It is assumed that slippage of the root-soil interface without root failure can occur only in limited cases, such as when the moisture content of the root-soil interface is high. However, to model both root failure and interface slippage, an interface-slippage model that can be applied to universal suction conditions is needed; hence, We focuses on developing a simple model for this objective, i.e., the MCV model. Notably, the present model can be combined with an elasto-plastic model for root-breakage by introducing a yield criterion and a flow in root domain.

The frictional coefficient is measured by conventional pullout tests. For instance, the frictional coefficient of the root-soil interfaces is 0.60 according to Section 2 and Tomobe et al., 2016).Fig. 12 maps the shear strength under different soil pressures and suctions, where the ranges of the x- and y-axis coverthe range of possible conditions under practical situations. Here, a soil pressure of < 10 kPa corresponds to grasslands and cultivated fields, where the depth of the rhizosphere is less than 1.0 m. Thus, the shear strength is primarily determined by suction, suggesting that the suction prevents slipping at interfaces between roots and cohesive soil.

Table 3
Model parameters of roots, soils and root-soil interfaces.

	Young's modulus (kPa)	Poisson's ratio	Penalty parameter (kN/m^3)	Frictional coefficient	a	b
Soil (S)	6038.9	0.35	–	–	–	–
Root (R)	60000.0	0.35	–	–	–	–
R-S interface	–	–	50000.0	0.60	1.91×10^{-1}	3.43×10^{-2}

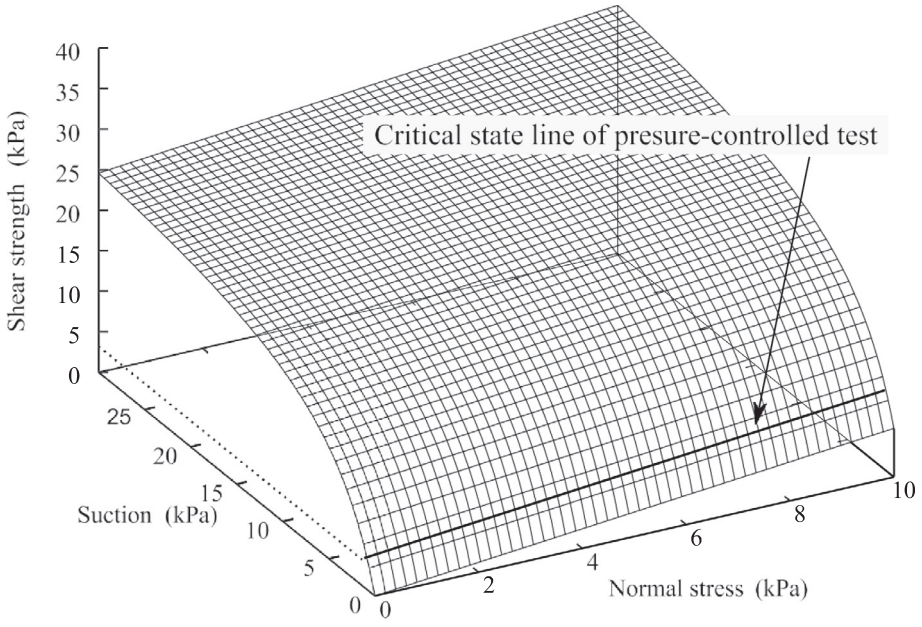

Fig. 12. Critical state surface of root-soil interface based on Mohr–Coulomb-Vilar model.

4.2. Implementation of MCV model based on NTS approach

Our model of the shear strength at the root-soil interfaces was numerically implemented by using the NTS approach (Simo et al., 1985; Wriggers, 2001; Puso et al., 2004; Wriggers 2006; Zavarise et al., 2009) within the FEM framework or predicting landslides in the presence of vegetation. This section summarizes the NTS approach in terms of root-soil contact problems and describes the implementation of suction-induced reinforcement in root-soil interfaces. The FEM has recently been applied to predict the mechanical behavior of rooted soil, thus providing an accurate analysis for root-soil interactions by using realistic root morphology. In this method, both the root and soil are discretized into FEs as depicted in Fig. 13, and the root-soil interfaces are established by a node-to-node (NTN) approach or line element (LE) scheme. However, developing a precise implementation for root-soil interfaces remains challenging. In this section, the NTS approach is applied to implement friction and suction-induced cohesion in the FEM analysis. The NTS approach is a widely-used method for expressing the mechanical interactions between deformable bodies in numerous engineering problems (Wriggers, 2006). This approcach utilizes a node on one body and a surface element on another body, as shown in Fig. 7. The NTS approach can express both slippage and separation at root-soil interfaces, which cannot be done by conventional NTN or LE methods. The governing equation and discretization of root-soil contact problems can be described as follow: Let us consider that a root and a soil mass are in contact, whith the contact surface identified as illustrated in Fig. 13. Under these conditions, the governing equation for the displacement field is given by the virtual work equation in Eqs. (1)–(4)

$$\delta W = \left(\int_\Omega \sigma \cdot \nabla \delta \mathbf{u} d\Omega - \int_\Omega \mathbf{f} \cdot \delta \mathbf{u} d\Omega - \int_\Gamma \mathbf{t} \cdot \delta \mathbf{u} d\Gamma \right)^r + \left(\int_\Omega \sigma \cdot \nabla \delta \mathbf{u} d\Omega - \int_\Omega \mathbf{f} \cdot \delta \mathbf{u} d\Omega - \int_\Gamma \mathbf{t} \cdot \delta \mathbf{u} d\Gamma \right)^s + \delta W^{rs} = 0, \tag{7}$$

where δW denotes the total virtual work, the superscripts r, s, and rs denote the root, soil and interfaces, respectively, $\sigma$is the Cauchy stress tensor, $\delta \mathbf{u}$ and $\nabla \delta \mathbf{u}$ are the virtual displacement and its gradient with respect to the current configuration, respectively; $\mathbf{f}$ is the gravitational forces and $\mathbf{t}$ is the traction forces. The last term denotes the virtual work

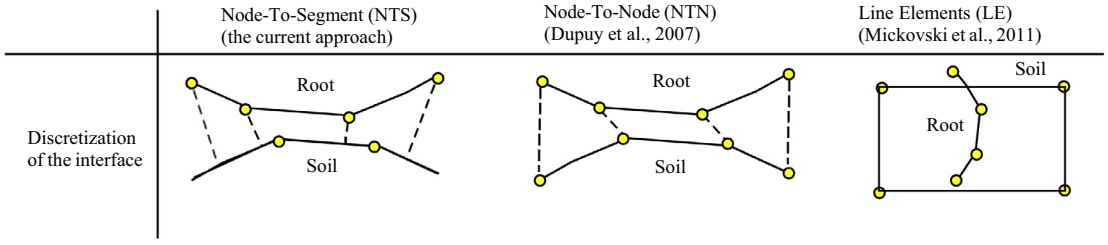

Fig. 13. Comparison among contact elements used in current and previous studies.

of the contact surface, which is explicitly expressed as Eq. (8):

$$\delta W^{rs} = \int \mathbf{t}_N \cdot \delta \mathbf{g}_N d\Gamma + \int \mathbf{t}_T \cdot \delta \mathbf{g}_T d\Gamma \tag{8}$$

where $\mathbf{t}_N$ and $\mathbf{t}_T$ are the normal and shear stress vectors, $\mathbf{g}_N$ is the gap vector from the soil surface to the closest point on the root surface and $\mathbf{g}_T$ is the tangential displacement from the initial contact point. Furthermore, a penalty parameter ϵ is introduced to prevent unnatural overlaps between roots and soil;

$$\mathbf{t}_N = \epsilon \cdot \mathbf{g}_N \tag{9}$$

Hence, the contact pressure is proportional to the degree of overlaps, which theoretically become zero when the penalty parameter is sufficiently large. The terms in the first and second parentheses within Eq. (7) are discretized by using finite elements and the last term is discretized by using the NTS elements, thus, the discretized equations are expressed by Eq. (10):

$$\delta W = \sum_{I=1}^{ne} \delta \mathbf{u}^{d(I)} \cdot \mathbf{R}^{d(I)} + \sum_{I=1}^{nc} \delta \mathbf{u}^{c(I)} \cdot \mathbf{R}^{c(I)} = 0 \tag{10}$$

where *ne* is the number of FEs for both the root and soil mass, *nc* denotes the number of NTS elements at the contact interfaces, and $\delta \mathbf{u}^{d(I)}$ and $\delta \mathbf{u}^{c(I)}$ are variations of the discretized displacement vectors for the bodies and the contact interfaces. $\mathbf{R}^{d(I)}$ is the residual vector for the domain, as derived in Eq. (3.63) in Wriggers (2006) and Hashiguchi and Yamakawa (2011). $\mathbf{R}^{c(I)}$ is the residual vector, which is derived in Eq. (9.20) in Wriggers (2006) and Eq. (23) and (62) in Zavarise and Lorenzis (2009). Because Eq. (10) is nonlinear for the displacement field, Newton method are employed as the solving algorithm, as presented in Fig. 14.

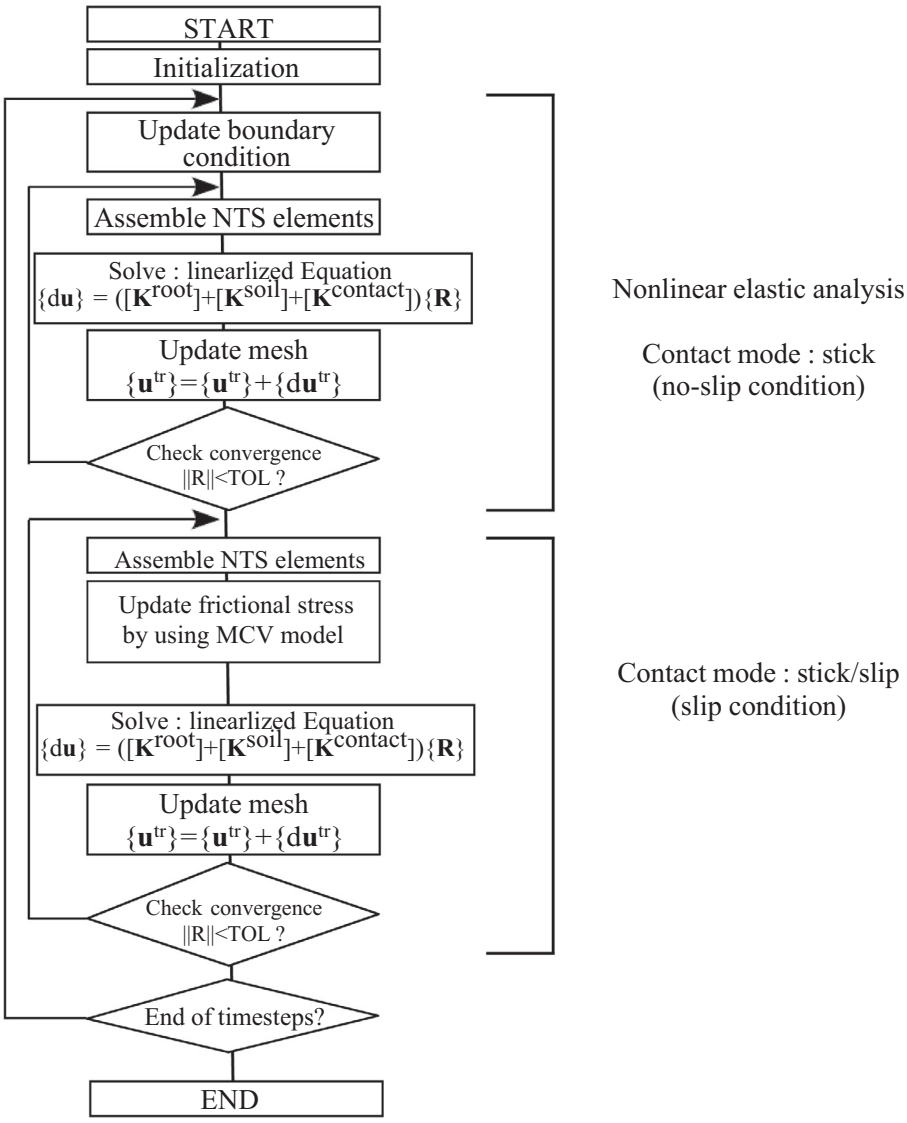

Fig. 14. Solution algorithm for current numerical simulation based on FEM and CCM.

4.3. Implementation of the suction-shear strength relationship

In this section, the NTS method is applied to the MCV model summarized in Section 4. In Eq. (8), the tangential gap is decomposed into two parts, i.e., the stick and slip:

$$\mathbf{g}_T = \mathbf{g}_T^{stick} + \mathbf{g}_T^{slip} \tag{11}$$

Here, $\mathbf{g}_T$ is the tangential gap between two material points on the contact surfaces, $\mathbf{g}_T^{stick}$ is the elastic part of the gap and $\mathbf{g}_T^{slip}$ is the plastic part. The shear stress $\mathbf{t}_T$ is expressed as Eq. (12).

$$\mathbf{t}_T = \epsilon \cdot \mathbf{g}_T^{stick} = \epsilon \cdot \left(\mathbf{g}_T - \mathbf{g}_T^{slip}\right) \tag{12}$$

This expression is derived by a natural assumption that the shear stress is caused by energy stored in the interface, which decays due to slippage. Hence, slippage reduces the shear stress. By introducing a penalty method, the shear stress increases with an increasing tangential gap when the stress is smaller than the frictional strength. Based on the MCV model of friction and suction-induced cohesion under unsaturated conditions, the slip criterion of the root-soil interfaces can be calculated as follows:

$$f = \|\mathbf{t}_T\| - c - \mu \cdot \|\mathbf{t}_N\| - \frac{s}{a \cdot s + b} \tag{13}$$

In case that f is positive, the increment of the slip $\dot{\mathbf{g}}_T^{slip}$ is updated by the flow rule as shown in Eq. (14),

$$\dot{\mathbf{g}}_T^{slip} = \dot{\lambda} \frac{\partial f}{\partial \mathbf{t}_T} \tag{14}$$

where $\dot{\lambda}$ is the increment of the plastic multiplier. Eqs. (12) – (14) are analogous to equations in the elasto-plasticity theory (Neto et al., 2011) and ensure that the direction of the slip is identical to the direction of shear stress. The increment in the slip $\dot{\mathbf{g}}_T^{slip}$ is integrated by employing the backward Euler scheme, where Eq. (14) is written as

$$\frac{\mathbf{g}_T^{slip}(t_{n+1}) - \mathbf{g}_T^{slip}(t_n)}{\Delta t} = \dot{\lambda} \frac{\partial f(t_{n+1})}{\partial \mathbf{t}_T^{tr}(t_{n+1})} \tag{15}$$

where t_n and t_{n+1} indicate the current and next subsequent time-step, respectively. By substituting Eq. (13) into Eq. (15) we obtain Eq. (16). Further, the superscript tr indicates the trial value, which is updated in the present operations.

$$\dot{\lambda} = \frac{\|\mathbf{t}_T^{tr}(t_{n+1})\| - \left(\mu \cdot \epsilon \cdot \|\mathbf{g}_N\| - \frac{s}{a \cdot s + b}\right)}{\epsilon \cdot \Delta t} \tag{16}$$

Therefore, the slip and shear stress are updated by Eq. (14).

$$\dot{\mathbf{g}}_T^{slip} = \frac{\|\mathbf{t}_T^{tr}(t_{n+1})\| - \left(\mu \cdot \epsilon \cdot \|\mathbf{g}_N\| - \frac{s}{a \cdot s + b}\right)}{\epsilon \cdot \Delta t} \frac{\partial f}{\partial \mathbf{t}_T^{tr}} \tag{17}$$

Eqs. (12), (13) and (17) are utilized in the solution algorithm as depicted in Fig. 14). A positive gap induces so-called adhesion, which prevents separation. Some models are available to introduce adhesion as presented by Fremond (1988). However, it is difficult to numerically formulate both the adhesion and cohesion; hence, the present paper focuses only on cohesion, with no adhesion. It is worth noting that when the two surfaces overlap, the gap is closed, which is indicated as a negative gap; in contrast, when the two surfaces are far apart, the gap is positive. In addition, the term cohesion is utilized herein as the strength with respect to the tangential direction based on the contact surface under zero normal stress in the MC failure criteria. In contrast, the adhesion is the strength in the normal direction of the contact surface (Wriggers, 2006) and describes the resistance force that is generated when two surfaces contact each other and then move apart.

5. Numerical simulation of pullout tests by the MCV-NTS approach

The objective of this section is to validate the accuracy of the current numerical approach based on the MCV model and NTS method by comparing our results with the experimental studies presented in Sections 2 and 3. Because the MCV-NTS approach models the shear strength of root-soil interfaces under changing soil pressure and suction, the validation presented in this section consists of two cases: (1) numerical simulations of the pullout tests of Tomobe et al. (2016) under varying soil pressure with a fixed suction and (2) suction-controlled pullout tests (see Section 3) performed at a constant soil pressure.

5.1. Mesh and boundary conditions

The mesh and boundary conditions of the pullout tests are shown in Fig. 15. The upper half of the specimen is modeled and each case simulates the process in which a root (8.0 cm × 0.05 cm) is pulled out from the soil specimen (6.0 cm × 2.0 cm) toward the left sides under the prescribed suction with normal pressure. The root diameter in the

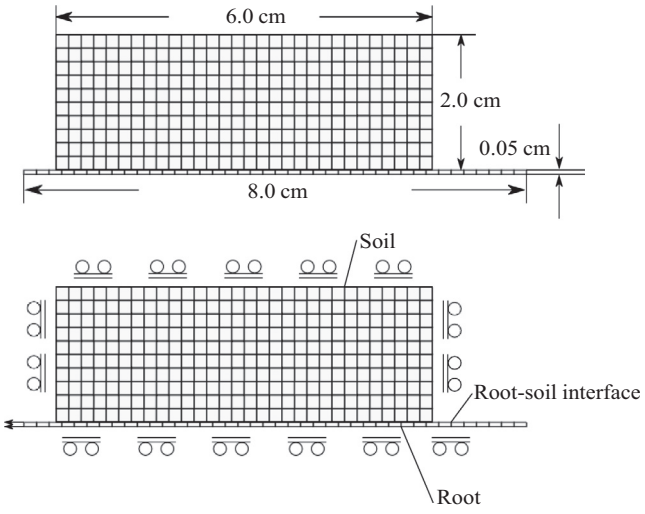

Fig. 15. Mesh and Boundary condition of numerical simulations for pullout test in latter sections.

numerical simulation is identical to the experimental value. Initial conditions are prepared by uniformly loading a downward displacement on the top of the soil domain, as shown in Fig. 15 for Case (1) which is the numerical simulation of Section 2. For Case (2), this step is ignored because the no vertical pressure was loaded in the suction-controlled pullout tests. For simplicity, the analysis was conducted under plane strain conditions, and the shear stress (kPa) on the root-soil interfaces was computed by dividing the pullout force (N) for the left side of the root by the contact area (m^2) of the specimen. Interestingly, the geometry of the numerical simulation is equivalent to a central plane with respect to the vertical section on the center of the root. Therefore, the numerical simulation is equivalent to the shear test along the root. Under these conditions, the relationship between shear displacement and shear stress is simulated, and the shear stress is computed by dividing the resistance force on the left side of the root by the contact area (unit depth), as the simulations assume plane strain conditions. Because the same constitutive models and governing equations hold for different scales and two dimensions (2D) or three dimensions (3D), the same constitutive model can be applied to both plane strain simulation results and 3D experimental results.

Both the roots and soil are assumed to be hyperplastic materials, and the root-soil interfaces are governed by the MCV equation presented in Section 4. As reported by Huang et al. (2012), the hyperelastic constitutive equation has been widely used to express the elastic behavior of biomaterials. However, the hyperelastic model cannot describe the viscosity, failure, or breakage of roots; therefore, the model should be utilized only when the root deformation is relatively small and no breakage occurs. A modified neo-Hookean elastic potential function presented by Vladimirov et al. (2008),Vladimirov et al., 2010 was utilized due to its simplicity, as we are focused on the interfacial behavior and as the deformation of the] roots and soil is relatively small. The present study utilized a hyperelastic constitutive equation and did not introduce plasticity for the bodies; thereby, both the roots and soil behave as elastic bodies. Although both the roots and soil are completely elasto-plastic materials in real situations, the bodies are modeled as elastic for the following reasons: (1) The present paper focuses on the interface model. (2) Shear strain is primarily localized at the interfaces. (3) It is technically difficult to perform a stable contact analysis when both of the materials are elasto-plastic. The Young modulus of the soil was obtained by unconfined compression tests (JIS A 1216), where the E_{50} value is utilized as Young modulus (6038.9 kPa), and the Young modulus of the roots was determined from the bending tests of soybean roots, which exhibit mechanical behavior similar to that of the barley roots. Among numerous methods for measuring the Young modulus of plants (Kim et al., 2008; Nazari et al., 2008; Ookawa et al., 2010; Liang et al., 2017), a bending test is selected due to its simplicity. The Young modulus is 60.0 MPa, and the Poissons ratio of the soil (0.35) was determined fromthe relationship between normal stress and horizontal stress during the pullout tests. For simplicity, the Poisson ratio of the roots is assumed to be the same as that of the soil. As shown in the Table 3, the frictional coefficient is 0.60, and parameters a and b are $1.91 \times 1.0^{-}1$ and $3.43 \times 1.0^{-}2$, respectively, which are given by the experiments in previous sections. The penalty parameter should be enough large and be small enough to avoid so-called ill-conditioning. The optional parameter $50,000 kN/m^3$ is identified by a parametric study.The model parameters of the MCV model, shown in Table 3, are consistent with those in Section 3.

Numerical simulations of the other pullout tests were performed as follows: For Case (1), pressured of 1.7, 3.6, 6.3, and 8.1 kPa were loaded by prescribing the equivalent displacement. The suction was not explicitly measured in previous research; instead, only the apparent cohesion was measured (3.14 kPa). Thus, the suction was estimated by using the MCV model and the measured parameters described in Section 3. Because the MCV-curve of the present root-soil interface is measured, it is possible to estimate thecohesion from the suction and vice versa. When the cohesion in Eq. (6) is 3.14 kPa, the suction is 0.27 kPa. Thus, the suction is estimated as 0.27 kPa. For simplicity in analysis, this suction value was usedfor all stress conditions, and it is assumed that the suction is almost the same for all cases. For Case (2), the suction-controlled pullout tests were simulated as follows: A suction of 0.5, 4.4, 5.8, 8.8, 22.0, or 28.0 kPa was applied, and the normal pressure is considered as 0 kPa. This condition was implemented via vertical fixing of the top of the soil-mesh, and followed by slight penetration (0.01 mm) at the root-soil interfaces under the initial condition. This technique is widely used to give a slight penetration prior to the contact simulation to avoid the divergence of the solution (Liu et al., 2003; Wriggers et al., 2006). When a contact simulation starts with no penetration under pseudo-static conditions, contact forces are suddenly loaded during the first Newton loop, which causes a severe ill-convergence problem in the penalty method. Therefore, the possible smallest penetration was introduced. Because there is no theoretical model to determine the exact value of the penetration, we executed the simulations more than 100 times and determine the specific value. Notably, the effect of the amount of penetration is negligible when the penetration is smaller than 0.01 mm.

5.2. Validation of the MCV-NTS approach

Fig. 16 compares the shear stress profile of the root-soil interface obtained from simulated and experimental pressure-controlled pullout tests. The simulation results are almost the same as the experimental results for all stress conditions. Although the initialangle of the simulated displacement-stress curve (initial displacement: 0–3 mm) is larger than the experimental value, the gap closes when

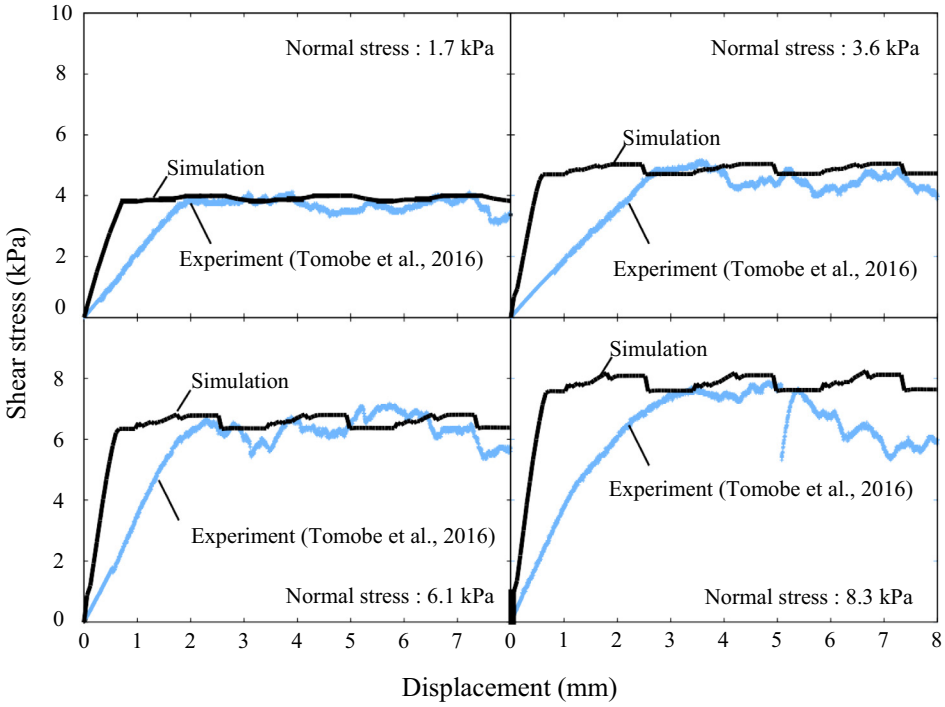

Fig. 16. Validation of simulation in comparison to experiments under pressure-controlled manner, where the suction is not changed.

slippage starts (displacement: 3–8 mm). Therefore, the MCV model and NTS approach can simulate slippage in root-soil interfaces under changing suction and soil pressure. It is worth noting that the Newton's method is converged under a tolerance (< 0.1 %) with respect to the relative L^2-norm of the residual vector. Oscillation patterns of the shear stress curve inevitably occurs when the NTS scheme is utilized with the penalty method as reported by Liu et al. (2003) and Wriggers et al. (2006).

The simulated contour of the deviatoric stress is shown in Fig. 17. Clearly, the deviatoric stress of the soil domain increases with increasing in soil pressure, which is an intuitively natural result. Further, the contour plot exihibits a different pattern for the suction-controlled results, as will be shown below.

Fig. 18 shows the relationship between displacement and shear strength for each suction value: (a) 0.5 kPa, (b) 4.4 kPa, (c) 5.8 kPa, (d) 8.8 kPa, (e) 22.0 kPa and (f) 28.0 kPa. In all cases, the simulated and experimental profiles are quantitatively similar, and the shear strength of the root-soil interfaces are almost the same. Consequently, the results suggest that the MCV-NTS approach can simulate the shear stress of root-soil interfaces under changing suction.

Fig. 19 presents a simulated contour map of the deviatoric stress for the pullout tests. From root to soil, the propagation of deviatoric stress is cut off when the suction is sufficiently small (suction: 0.5 kPa). For a suction value of 28.0 kPa, the deviatoric stress of soil is significantly larger and is continuously distributed across the root-soil interface. In both cases, the deviatoric stress increases with increasing shear displacement; however, the mechanical characteristics of two cases are different.For a suction of is 0.5 kPa, the increase in deviatoric stress stops when the

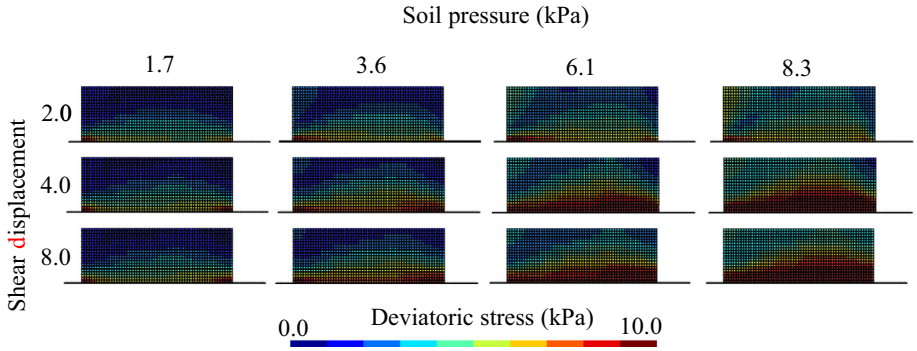

Fig. 17. Contour map of deviatoric stress of soil and root domains. The shear stress of soil domain increases with the increase of soil pressure.

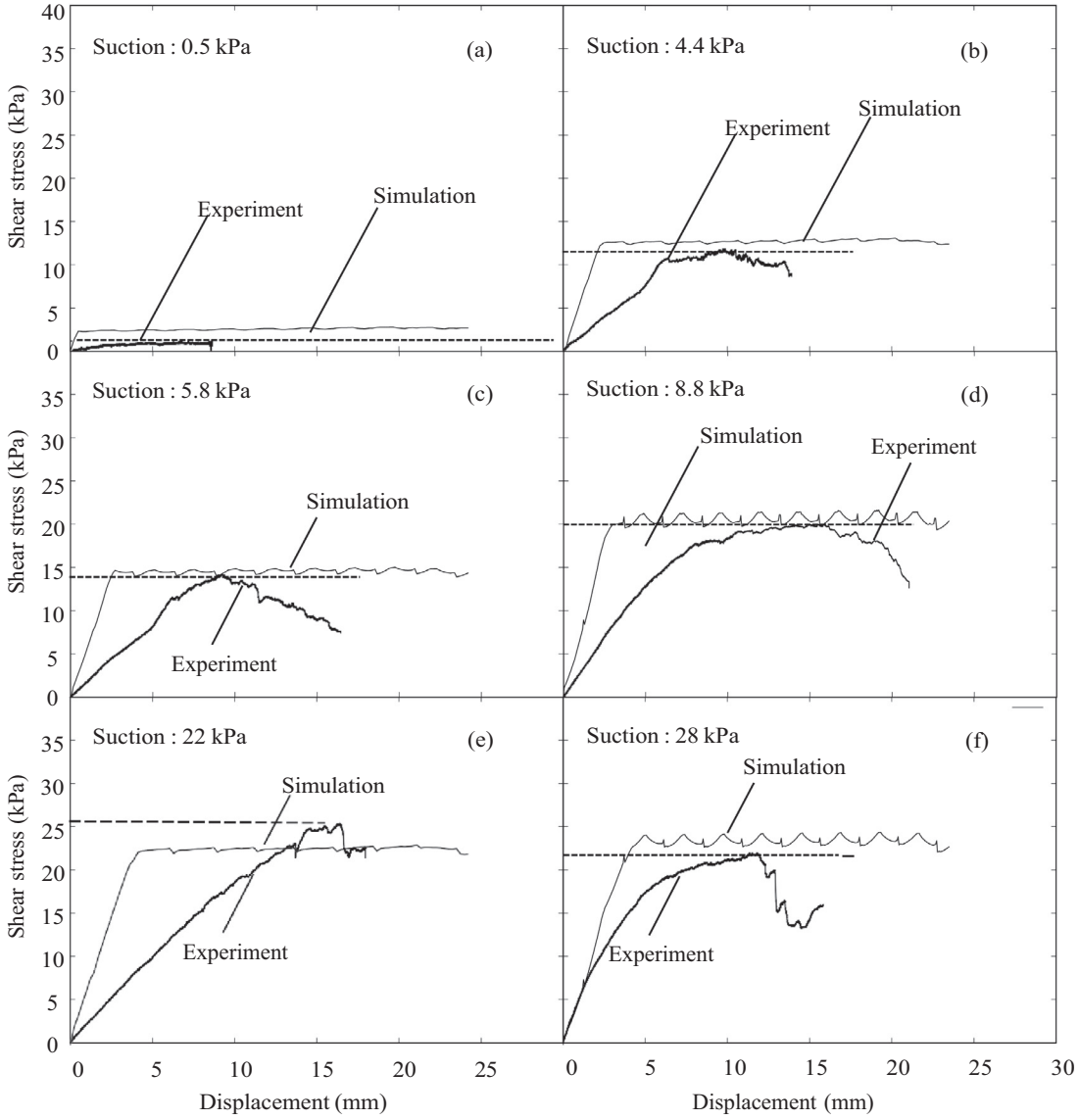

Fig. 18. Validation of simulation in comparison to the experiments under suction-controlled condition, where the soil pressure is not changed.

shear displacement reaches 2.0 mm. By contrast, the increase in the deviatoric stress continues for a suction of 28.0 kPa.

Although the contour maps shown in Figs. 17 and 19 are similar, the contour lines of the deviatoric stress in Fig. 19 are parallel to each other and symmetric with respect to the center of the figure. By contrast, the contour lines in Fig. 17 are more complex and asymmetrical. This difference can be explained as follows: The suction-induced cohesion is independent of the stress field, therefore, under low-soil-pressure conditions, the shear stress of root-soil interfaces is uniformly distributed. However, the soil-pressure-induced friction depends on the stress field of both the soil and roots, and the deformation of the roots and soil in the right sides differs from that on the left side, thereby resulting in the complexity and asymmetry. It is considered that this difference in the stress-contours will be helpful for other applications, such as creating simpler and semi-empirical models for the pull-out resistance of a single root.

Above all, these results indicate that the MCV model can reproduce the experimentaly observed shear strength of root-soil interfaces as a function of normal stress and suction. This model can also provide accurate simulations of pullout tests under different suction conditions, which has not been previously presented. It is worth noting that each experiment is conducted under constant hydraulic conditions; hence, this model can be consistently applied to a range of dry to wet conditions only if the suction varies monotonically. Moreover, this model cannot predict the effect of hysteresis. The MCV-NTS approach is compatible with any FEM scheme if one uses elements based on linear interpolation function, such as three-node triangle or four-node rectangle elements. In addition, because the NTS formulation is suitable for both 2D and 3D analysis, it is expected that the MVC-NTS scheme can be applied to

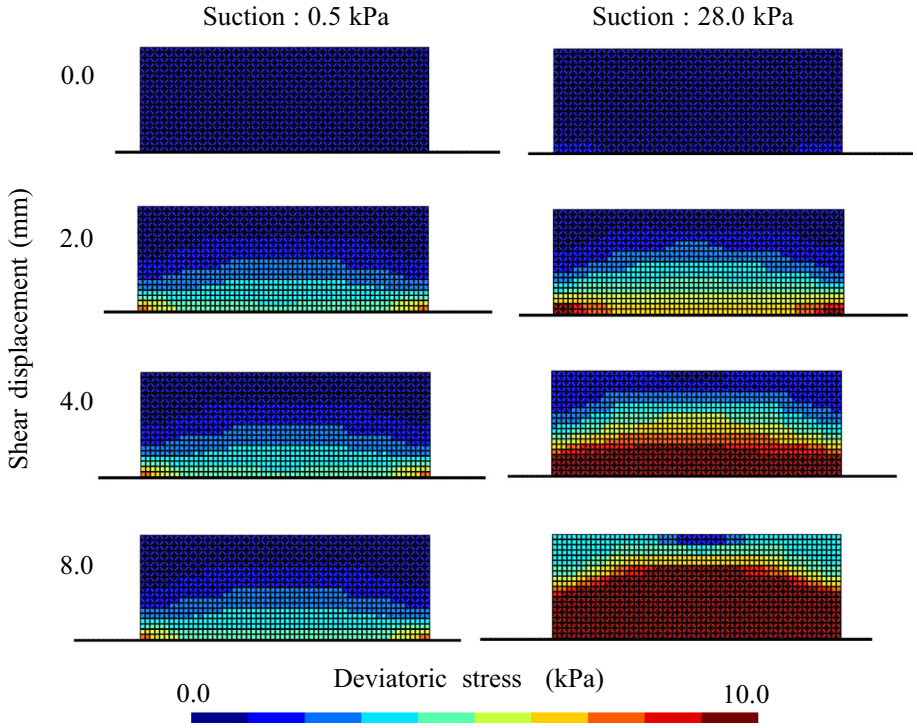

Fig. 19. Contour map of deviatoric stress of soil and root domains. Shear stress of soil domain increases with the increase of suction.

root-soil contact problems under 3D conditions to simulate the deformation of rooted soil under prescribed suction conditions. The present model overestimates the stiffness, due to the mathematical and numerical charcteristics of the penalty method (Wriggers, 2006). The stiffness of the displacement-shear stress curve is governed by the penalty parameter which is not a material parameter but a numerically determined parameter. Future studies will introduce constraint conditions to introduce softening to the shear-stiffness curve based on the subloading-surface model (Hashiguch and Yamakawa, 2013).

6. Pullout resistance of root under changing pressure/suction by MCV-NTS approach

The objective of this numerical experiment was to investigate the applicability of the MCV-NTS approach. Here root pullout from soils was simulated under dynamic suction conditions for different soil pressures in order to test (1) whether the numerical simulation can continuously predict the shear stress of root-soil interfaces under dynamic suction conditions, and (2) whether the simulation can perform well under realistic and unconfined conditions of shallow soil depth. The problem described in this section is designated to demonstrate the pullout behavior of roots from the soil, as illustrated in Fig. 1 under conditions that are more realistic than those consideredin the previous sections.

6.1. Boundary conditions and suction control

From this standpoint, we simulated three cases in which the soil pressures are equivalent to those at soil depths of 30, 60, and 90 cm. These soil pressures were computed from the bulk density (1.28 g/cm^3) of the soil sampling site (Table 2), and were loaded as a pre-stress. For each case, a root is pulled out from the soil for 1.6 cm, and the suction is set at 28.0 kPa while the shear displacement is 0.0–0.6 cm, at which pointthe roots start to slip. A suction of 28.0 kPa was selected for the following reasons: (1) The simulateddrying process is appropriate for evaluating the applicability of the MCV-NTS scheme due to the dynamically changing suction. (2) The suction-induced cohesion is almost maximized for the suction in the present combination of roots and soil, hence, the suction significantly declines. The conditions for the simulation are as follows. Initially, the suction is set at 28 kPa. As root extraction begins, the shear stress increases and eventually reaches its peak. When the shear stress reaches its peak, slippage occurs in the shear plane. In this simulation, between the point at which the interface slips completely and the shear displacement reaches 0.6 cm and the point at which the shear ends and the shear displacement reaches 1.6 cm, the suction decreases according to the following function

$$s = -(22.5)(u - u_s) + 28.0 \quad (u_s \leqslant u \leqslant 1.6), \tag{18}$$

where s is the suction (kPa), u is the shear displacement (cm) and u_s(=0.6 cm) is the displacement when the suction starts to decrease.

It is expected that the stress state of the root-soil interface is within the MCV slip surface under the initial condition and then moves to the MCV slip surface, remaining there until the suction changes; afterward, the stress state moves along the MCV slip surface as the dynamic suction decreases. The mesh and boundary conditions are identical

to those in Section 5, and the pre-stress is set such that the soil pressure is the same as that for a depth of 0.3, 0.6, or 0.9 m at the sampling site. In the numerical simulation, prior to the pull-out process, a soil pressure corresponding to a depth of 30 to 90 cm is loaded, therefore, the equivalent pre-stress represents different soil-pressures. These depth are utilized because the roots are distributed at depth of 0.0–1.0 m at the sampling site and similar conditions are reproduced in the simulation. The material parameters of the simulation are shown in Table 3, as obtained from the experiment described in Section 3, which is consistent with Section 5.

6.2. Demonstration of pullout behavior under dry-to-wet conditions

Fig. 20 shows the stress-path of the simulation for the three cases. Fig. 20(a) shows the slip criterion of the MCV model which represents the shear strength for a given soil pressure and suction. Figs. 20(b) and (c) display the pathway of the shear stress in relation to the suction and soil pressure, respectively. Fig. 20 (d) shows that the soil pressure is primarily fixed for each case and that the suction changes during the pullout process. As shown in the Fig. 20 (b), the stress state of the root-soil interface is within the MCV slip surface under the initial conditions and then moves to the MCV slip surface, remaining at the same point until the suction changes; afterward, the stress state moves along the hyperbolic curve of the MCV model as the suction decreases, which is consistent with the MCV model. The shear strength for a depth of 90 cm is greater than that for 30 cm, which reflects the contribution of friction, in agreement with the MCV model and pullout experiments. According to Fig. 20 (c), the stress state of the root-soil interface in this case is also within the MCV slip surface under the initial conditions; subsequently, the stress statemoves to the MCV slip surface and remains at the same point until the suction changes. After the suction starts to decrease, the MC values decrease due to the decline in suction-induced cohesion, which is consistent with the MCV model and suction-controlled pullout tests. The above relationship is illustrated in Fig. 20 (a), along with shear stress profile and the MCV surface.

Fig. 21 presents the shear stress-displacement curve, suction-displacement curve, soil pressure–displacement curve, and stress contour of the deviatoric stress. As the displacement increases, the shear stress of the root-soil interface reaches the shear strength defined by the MCV model. At failure, which indicates the onset of slipping, the displacement increases under the same shear stress. The shear stress for a depth of 90.0 cm is greater than that for of 30.0 cm, which reflects the contribution of friction-induced by soil pressure. The soil pressure profile is shown in the lower left region of the figure, where the soil pressure remains nearly constant for each case in the numerical experiment. When the displacement reaches 0.6 cm, the suction is artificially reduced, indicating that the root-soil interface is gradually moistened. The reduced suction lessens the suction-induced cohesion, which results in a

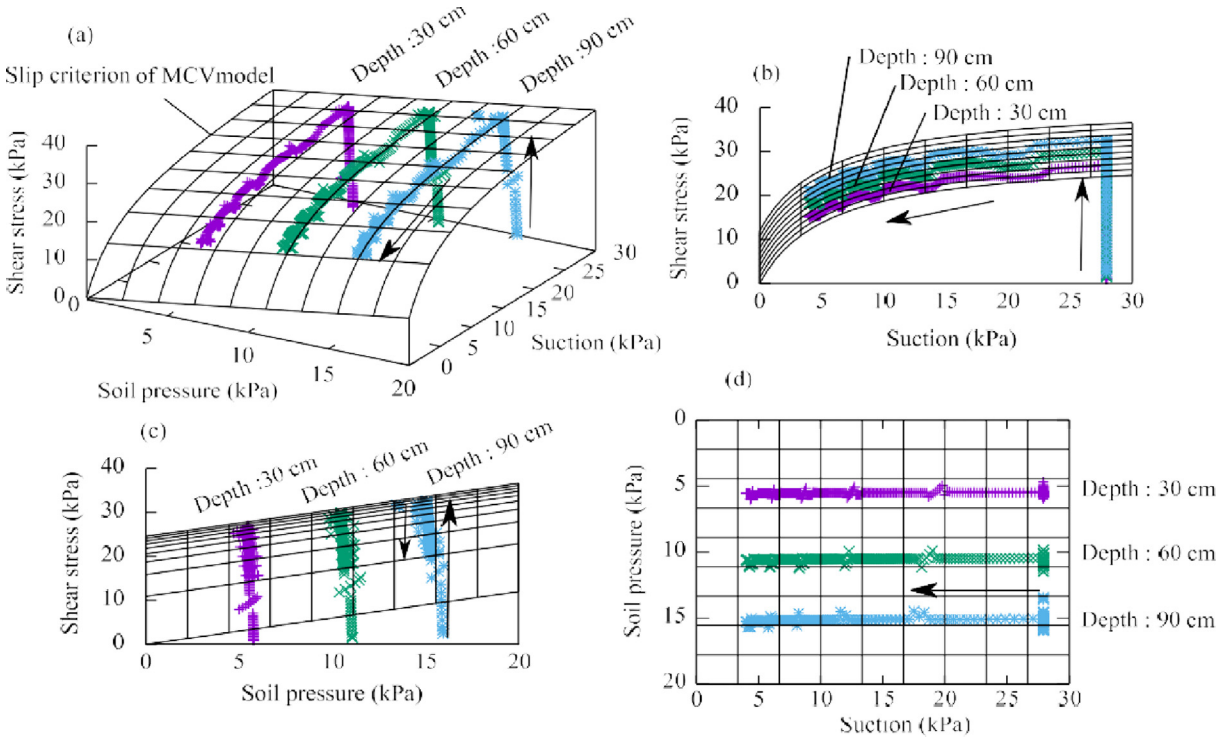

Fig. 20. Stress path plotted with MCV surface under dynamic suction conditions for different soil pressure conditions. The soil pressures are equivalent to those of the depth of 30.0, 60.0 and 90.0 cm from the ground surfaces.

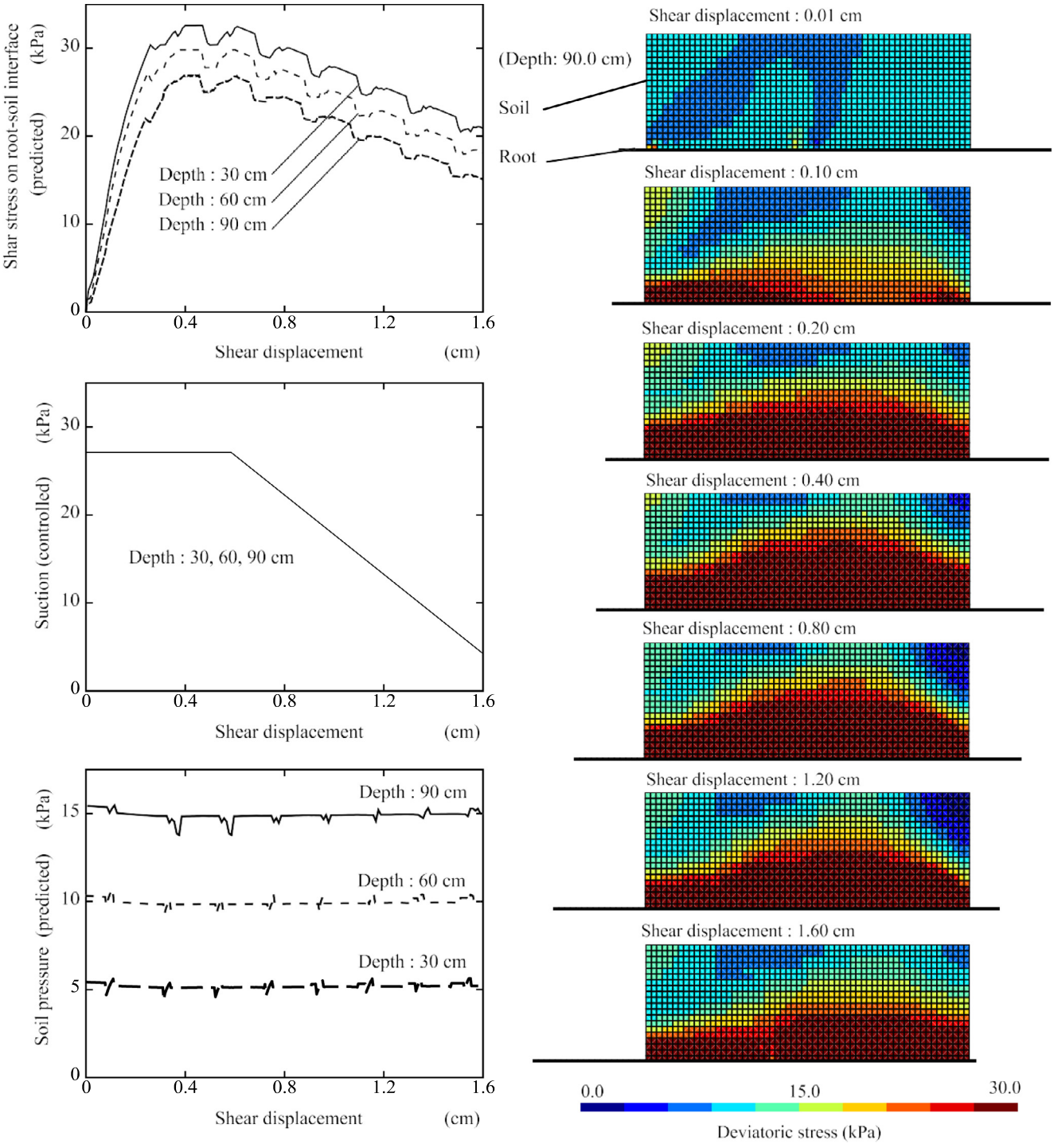

Fig. 21. Profiles of shear stress of root soil interfaces and deviatoric stress of root and soil.

decreased shear stress during slippage. The right side of the figure shows the contour map of the deviatoric stress for both the root and soil domains. The deviatoric stress at the bottom of the soil domain increases as the displacement increases from 0.01 to 0.20 cm; subsequently, the stress contour maintains the same color as the displacement increases from0.20 to 0.80 cm. Afterward, the zone of deviatoric stress $\geqslant$30.0 kPa shrinks as time passes, due to the decrease in the suction. Although a slight oscillation of the solution is observed, the degree of oscillation is small from the standpoint of practical use.

Another key point is shown by the topology of the deviatoric stress contour in Fig. 21. Here, the profile of the contour is similar to those for the simulated soil-pressure-controlled pullout tests, where the soil-pressure-induced friction is dominant. In fact, the gradient of this contour

is enhanced and more complex, indicating that the friction induces spatial complexity in the stress field and that the suction-induced cohesion enhances the spatial complexity.

As demonstrated by these results, the NTS-MCV approach can provide a reasonable solution for root-soil contact problems under dynamically changing suction for different types of soil. These results indicate that the current approach can be applied to root-soil contact problems and provides a consistent solution based on the MCV model. The proposed approach enhances the accuracy for the numerical simulations of deformation in rooted soil based on FE analysis (Dupuy et al., 2007; Rahardjo et al., 2009; Mickovski et al., 2011). In addition, our model can simulate simple wet-to-dry processes or dry-to-wet processes with ease. However, the applicability for wet-dry cycles is not demonstrated in this work. In future studies, shear tests for root-soil interfaces will be conducted under cyclic wet-dry conditions, to investigate the applicability of the MCV model. under these conditions.

7. Conclusion

The current paper demonstrates that the MCV model and NTS approach can successfully simulate the deformation and shear strength of rooted soil. The following conclusions can be drawn.

A novel pullout apparatus has been developed to measure the suction-induced cohesion of root-soil interfaces. The results show that the suction-induced cohesion increases with increasing suction for a suction range of 0 to 10 kPa, reaching 25 kPa, which exceeds the contribution of friction under low-confirming conditions, such as those found in the topsoil of grasslands or slopes. Both suction-induced cohesion and friction were modeled using the MCV model, which combines the MC slip criterion as a friction model and the Vilar model (Vilar, 2006) for suction-induced cohesion. This model can reproduce the shear strength of root-soil interfaces as a function of normal stress and suction. The MCV model has been implemented for the first time using the NTS approach. The MCV model was introduced as the slip criterion and slip rule, and corresponding variables were updated by a return-mapping scheme. The model increases the shear strength of the NTS elements with increasing suction and increasing normal stress. Therefore, the shear stress of the root-soil interfaces is affected by both hydraulic and mechanical conditions. Such models have not been previously used for root-soil contact problems. As shown in Sections 5 and 6, the MCV model was utilized to predict the shear strength of root-soil interfaces under dynamic suction conditions, which is difficult to predict via the conventional models, such as those described by Mickovski et al. (2010), Schwarz et al. (2011), and Tomobe et al. (2016),Tomobe et al., 2019.

The current simulation method was validated by simulating pullout tests under controlled pressure and suction. The results show that the current model and implementation can accurately reproduce the relationship between shear stress and displacement for both pressure-induced friction and suction-induced cohesion. The results also predict the deviatoric stress under different suction levels. Our findings suggest that the propagation of shear stress from the roots to the soil is cut off when the suction reaches almost zero; moreover, the shear stress continuously propargates as the suction increasesbecause the deviatoric stress distribution can change due to the presence of suction-induced cohesion at the root-soil interface.

A numerical root pullout experiment was performed to evaluate the applicability of this model to dynamic suction conditions in which the suction of the root-soil interfaces varies during the pullout process. The results indicate that the NTS-MCV approach can provide reasonable solutions for root-soil contact problems under dynamically changing suction for different types of soils. These findings show that the current approach can be applied to root-soil contact problems and provides a consistent solution based on the MCV model. Accurate modeling of the shear strength of root-soil interfaces under changing soil pressure and suction is needed to solve root-soil contact problems based on the FEM (Dupuy et al., 2007; Rahardjo et al., 2009; Mickovski et al., 2010), and the proposed method offers a series of experimental, modeling, and implementation approaches to better understand the root-soil-interface-associated dynamics of vegetated slopes.

Declaration of Competing Interest

The authors declare that they have no known competing financial interests or personal relationships that could have appeared to influence the work reported in this paper.

Acknowledgments

The work was supported by Grant-in-Aid for JSPS Research Fellow Number 17J02383and Grant-in-Aid for Young Scientists (Start-up) Number 20K22599.

References

Abe, K., Ziemer, R.R., 1991. Effect of tree roots on a shear zone: modeling reinforced shear stress. Can. J. For. Res. 21, 1012–1019.

Bischetti, G.B., Chiaradia, E.A., D'Agostino, V., Simonato, T., 2010. Quantifying the effect of brush layering on slope stability. Ecol. Eng. 36, 258–264.

Dupuy, L.X., Fourcaud, T., Lac, P., Stokes, A., 2007. A generic 3D finite element model of tree anchorage integrating soil mechanics and real root system architecture. Am. J. Bot. 94, 1506–1514.

Eab, K.H., Likitlersuang, S., Takahashi, A., 2015. Laboratory and modelling investigation of root-reinforced system for slope stabilisation. Soils Found. 55, 1270–1281.

Endo, T., 1980. Effect of tree roots upon the shear strength of soil. For. For. Prod. Res. Inst. 14, 112–115.

Ghavami, K., Toledo Filho, R.D., Barbosa, N.P., 1999. Behaviour of composite soil reinforced with natural fibres. Cem. Concr. Compos. 21, 39–48.

Giadrossich, F., Stokes, A., Schwarz, M., Cohen, D., Cislaghi, A., Vergani, C., Hubble, T., Phillips, C., 2017. Methods to measure the mechanical behaviour of tree roots: A review. Ecol. Eng. 109, 256–271.

Hejazi, S.M., Sheikhzadeh, M., Abtahi, S.M., Zadhoush, A., 2012. A simple review of soil reinforcement by using natural and synthetic fibers. Constr. Build. Mater.

Huang, R., Becker, A.A., Jones, I.A., 2012. Modelling cell wall growth using a fibre-reinforced hyperelasticviscoplastic constitutive law. J. Mech. Phys. Solids 60, 750–783.

Ibraim, E., Diambra, A., Muir Wood, D., Russell, A.R., 2010. Static liquefaction of fibre reinforced sand under monotonic loading. Geotext. Geomembranes 28, 374–385.

Ji, X., Cong, X., Dai, H., Zhang, A., Chen, L., 2018. Studying the mechanical properties of the soil-root interface using the pullout test method. J. Mt. Sci. 15, 309–322.

Jin, K., Wang, H., Tao, J., Du, D., 2019. Mechanical analysis and progressive failure prediction for fibre metal laminates using a 3D constitutive model. Compos. Part A Appl. Sci. Manuf. 124, 105490.

Jotisankasa, A., Rurgchaisri, N., 2018. Geotextiles and Geomembranes Shear strength of interfaces between unsaturated soils and composite geotextile with polyester yarn reinforcement. Geotext. Geomembranes 46, 338–353. https://doi.org/10.1016/j.geotexmem.2017.12.003.

Kim, G.-W., Kim, M.-S., Do, G.-S., Kang, S.-W., Lee, S.-H., Sagara, Y., Lee, I.-B., Bae, Y.-H., 2008. Determination of the Viscoelastic Properties of Apple Flesh under Quasi-Static Compression Based on Finite Element Method Optimization. Food Sci. Technol. Res. 14, 221–231.

Leung, A.K., Garg, A., Ng, C.W.W., 2015. Effects of plant roots on soil-water retention and induced suction in vegetated soil. Eng. Geol. 193, 187–197.

Liang, T., Bengough, A.G., Knappett, J.A., MuirWood, D., Loades, K. W., Hallett, P.D., Boldrin, D., Leung, A.K., Meijer, G.J., 2017. Scaling of the reinforcement of soil slopes by living plants in a geotechnical centrifuge. Ecol. Eng. 109, 207–227.

Likos, W.J., Wayllace, A., Godt, J., Lu, N., 2018. Modified Direct Shear Apparatus for Unsaturated Sands at Low Suction and Stress 33, 286–298.

Liu, W.N., Meschke, G., Mang, H.A., 2003. Algorithmic stabilization of FE analyses of 2D frictional contact problems with large slip. Comput. Methods Appl. Mech. Eng. 192, 2099–2124.

Mahannopkul, K., Jotisankasa, A., 2019. Influences of root concentration and suction on Chrysopogon zizanioides reinforcement of soil. Soils Found. 59, 500–516.

Mickovski, S.B., Stokes, A., Beek, R. Van, Ghestem, M., Fourcaud, T., 2011. Simulation of direct shear tests on rooted and non-rooted soil using finite element analysis. Ecol. Eng. 37, 1523–1532.

Nazari, G.M., Jafari, A., Mohtasebi, S.S., Tabatabaeefar, A., Sharifi, A., O'Dogherty, M.J., Rafiee, S., Richard, G., 2008. Effects of moisture content and level in the crop on the engineering properties of alfalfa stems. Biosyst. Eng. 101, 199–208.

Ng, C.W.W., Woon, K.X., Leung, A.K., Chu, L.M., 2013. Experimental investigation of induced suction distribution in a grass-covered soil 52, 219–223.

Ni, J.J., Leung, A.K., Ng, C.W.W., Shao, W., 2018. Modelling hydro-mechanical reinforcements of plants to slope stability 95, 99–109.

Ni, J.J., Leung, A.K., Ng, C.W.W., 2019. Unsaturated hydraulic properties of vegetated soil under single and mixed planting conditions. Geotechnique 69 (6), 554–559.

Ookawa, T., Hobo, T., Yano, M., Murata, K., Ando, T., Miura, H., Asano, K., Ochiai, Y., Ikeda, M., Nishitani, R., Ebitani, T., Ozaki, H., Angeles, E.R., Hirasawa, T., Matsuoka, M., 2010. New approach for rice improvement using a pleiotropic QTL gene for lodging resistance and yield. Nat. Commun. 1 (8), 1–11.

Pallewattha, M., Indraratna, B., Heitor, A., Rujikiatkamjorn, C., 2019. Shear strength of a vegetated soil incorporating both root reinforcement and suction. Transp. Geotech. 18, 72–82.

Schwarz, M., Cohen, D., Or, D., 2011. Pullout tests of root analogs and natural root bundles in soil: Experiments and modeling. J. Geophys. Res. 116, 1–14.

Simo, J.C., Wriggers, P., Taylor, R.L., 1985. A perturbed Lagrangian formulation for the finite element solution of contact problems. Comput. Methods Appl. Mech. Eng. 50, 163–180.

Song, L., Li, J.H., Zhou, T., Fredlund, D.G., 2017. Experimental study on unsaturated hydraulic properties of vegetated soil 103, 207–216.

Sugiman, S., Crocombe, A.D., Katnam, K.B., 2011. Investigating the static response of hybrid fibre-metal laminate doublers loaded in tension. Compos. Part B Eng. 42, 1867–1884.

Tomobe, H., Fujisawa, K., Murakami, A., 2016. Shear tests and modeling of root-soil contact interface by using novel pullout test. IDRE J. 84, 223–232.

Tomobe, H., Fujisawa, K., Murakami, A., 2019. Experiments and FE-analysis of 2-D root-soil contact problems based on node-to-segment approach. Soils Found. in press.

Vilar, O.M., 2006. A simplified procedure to estimate the shear strength envelope of unsaturated soils. Can. Geotech. J. 43, 1088–1095.

Vladimirov, I.N., Pietryga, M.P., Reese, S., 2008. On the modelling of non-linear kinematic hardening at finite strains with application to springback-comparison of time integration algorithms. Int. J. Numer. Methods Eng. 75, 1–28.

Vladimirov, I.N., Pietryga, M.P., Reese, S., 2010. Anisotropic finite elastoplasticity with nonlinear kinematic and isotropic hardening and application to sheet metal forming. Int. J. Plast. 26, 659–687.

Voottipuex, P., Bergado, D.T., Mairaeng, W., Chucheepsakul, S., Modmoltin, C., 2008. Soil reinforcement with combination roots system: A case study of vetiver grass and Acacia Mangium Willd. Lowl. Technol. Int. 10, 56–67.

Wijaya, M., Leong, E.C., Rahardjo, H., 2015. Effect of shrinkage on air-entry value of soils. Soils Found. 55 (1), 166–180.

Wriggers, P., 2006. Computational contact mechanics, 2nd ed. Springer. Springer, Berlin Heidelberg, Berlin, Heidelberg.

Zavarise, G., Lorenzis, L.D., 2009. A modified node-to-segment algorithm passing the contact patch test. Int. J. Numer. Methods Eng. 79, 379–416.

Zhang, L.L., Fredlund, D.G., Fredlund, M.D., Ward Wilson, G., 2013. Modeling the unsaturated soil zone in slope stability analysis. Can. Geotech. J. 51, 1384–1398.